Geoderma 371 (2020) 114380

Contents lists available at ScienceDirect

Geoderma

journal homepage: www.elsevier.com/locate/geoderma

Transformation of clay minerals in salt-affected soils, Pantanal wetland, Brazil

Gabriel Ramatis Pugliese Andrade[a,*], Sheila Aparecida Correia Furquim[b], Thiago Tavares Vidoca do Nascimento[c], Alex Cordeiro Brito[b], Gabriela Ribeiro Camargo[b], Giovanna Cristina de Souza[b]

[a] Soil Laboratory (LSOL-CCTA), Universidade Estadual do Norte Fluminense Darcy Ribeiro (UENF), Avenida Alberto Lamego, 2000, Campos dos Goytacazes, RJ 28013-602, Brazil
[b] Department of Environmental Sciences, Universidade Federal de São Paulo (UNIFESP), Rua São Nicolau, 210, Centro, Diadema, SP 09913-030, Brazil
[c] Department of Geography, Universidade de São Paulo (USP), Av. Lineu Prestes, 338, Cidade Universitária, São Paulo, SP 05508-000, Brazil

ARTICLE INFO

Handling editor: Yvan Capowiez

Keywords:
Mixed-layered minerals
Solonization
Solodization
Saline soils
Sodic soils

ABSTRACT

Some of the saline lakes occurring in the Nhecolândia, a sub-region of the Pantanal wetland, have transformed into brackish lakes due to atypical freshwater input from seasonal flooding. Consequently, the Saline-Sodic soils formed around the saline lakes, previously submitted to salinization and solonization, have been converted into Sodic, Solodized-Solonetz and Solod soils around the brackish lakes, under the action of solonization and/or solodization. In this research, fine clay fractions (< 0.2 μm size) of B natric horizons of Saline-Sodic soils surrounding a saline lake and Sodic and Solod soils surrounding brackish lakes were studied in order to understand the genesis of clay minerals with the gradual transformation of these salt-affected soils. Fine clay mineralogy was studied by experimental XRD, full XRD profile modelling using NEWMOD 3.2.1, STEM/HAADF and ICP-OES. In the Saline-Sodic soils, illitic mixed-layered R0 kaolinite-illite (K-I) and R0 illite-smectite (I-S) comprise most of the samples, the percentage of illite (in K-I and I-S), kaolinite in R0 kaolinite smectite (K-S and K-I), and smectite (in K-S and I-S) layers was 73–76%, 14–16% and 10–11%, respectively. In the Sodic soils, illitic K-I and/or I-S still dominate the samples, but the percentage of illite layers (in K-I, I-S and/or illite-vermiculite) is smaller (52–68%), with an increase of kaolinite (19–35% in end member kaolinite, K-S and K-I) and smectite (7–21% in K-S and I-S) layers. Finally, the Solod soil shows dominance of smectitic I-S and illitic I-S, with a significant decrease in illite layers (36–41% in K-I and I-S), the maintenance of kaolinite layers (21–31% in pure kaolinite, K-S and K-I) and significant increase in smectite layers (31–37% in K-S and I-S). These progressive changes in mineral assemblages from the most alkaline (Saline-Sodic) to the most acidic soil (Solod) is probably due to gradual transformations, especially from the illitic phases, neoformed around the saline lake, to other 2:1 (mixed-layered smectite) and 1:1 (mixed-layered kaolinite) clay minerals under the new geochemical conditions of the brackish lakes. The mineral range observed in the samples suggest that the transformation from one clay mineral into another takes place without the complete dissolution and consequent precipitation, but as progressive mixed-layering reactions. This model explains the existence of several mixed-layered minerals, which is in agreement with the geochemical evolution of soils under progressive solonization and solodization.

1. Introduction

Solonization is the process that involves Na^+ accumulation in the soil exchangeable complex, increasing the ratio of Na^+ to other adsorbed cations (Gedroiz, 1925; Schaetzl and Anderson, 2005). It is mainly responsible for the formation of Sodic soils (Solonetzes), which are generally characterized by exchangeable sodium percentage (ESP) of ≥15%, sodium adsorbed ratio (SAR) ≥13, electrical conductivity (EC) < 4 dS m^{-1} and pH ≥ 8.5 (USSSL, 1954; Sparks, 2003). The low EC is explained by the relatively small presence of bivalent cations and the high pH is related to high ESP and SAR, inasmuch as alkaline pH commonly occurs due to the major release of OH^- by Na^+ carbonate

* Corresponding author.
E-mail address: gabriel.andrade@uenf.br (G.R.P. Andrade).

https://doi.org/10.1016/j.geoderma.2020.114380
Received 15 August 2019; Received in revised form 10 March 2020; Accepted 6 April 2020

dissolution (McBride, 1994) and Na^+ hydrolysis (Fanning and Fanning, 1989; Bohn et al., 2001).[1] These characteristics can reach the whole profile but are more intense in the B natric (Bn) horizon, which tends to present hard consistency and low hydraulic conductivity because of the clay dispersion provoked by the sodic environment (Levy et al., 1998).

Saline-Sodic soils, characterized by ESP ≥ 15%, SAR ≥ 13 and EC ≥ 4 dS m^{-1}, are also affected by solonization, but in association with the salinization process. Salinization is the accumulation of salts more soluble than gypsum, being responsible for high amounts of exchangeable mono and, especially, bivalent cations, which is expressed by high EC values. Solonization, such as in the Sodic soils, accounts for an important accumulation of exchangeable Na^+ in comparison to the other cations, promoting significant increase of ESP and SAR in these soils (USSSL, 1954; Sparks, 2003). The values of pH tend to be < 8.5, but vary according to the ratio of Na^+ to other exchangeable cations, such as Ca^{2+} and Mg^{2+}. Higher presence of these bivalent cations prevents hydrolysis and maintains lower pH values (Bohn et al., 2001).

When Saline-Sodic soils are submitted to leaching, solonization tends to become the main process and Sodic Soils are generally formed. If the leaching continues, solonization is commonly replaced by solodization, a process that leads to Na^+ depletion and the concomitant increase of Al^{+3} and H^+ in the exchangeable complex (Gedroiz, 1925; Schaetzl and Anderson, 2005). Solodized-Solonetz and Solod are formed by solodization in intermediate and terminal leaching conditions, respectively (Schaetzl and Anderson, 2005). In both of these soils, also called degraded Sodic soils, EC is maintained < 4 dS m^{-1} and SAR decreases to values < 13, but the ESP and pH are usually ≥10% producing neutral to slightly alkaline (6.5–8.5) soil in the former and < 10% a more acidic in the latter. The leaching conditions are more intense in the upper horizons of Solodized-Solonetzes and are extended to the B and C horizons in Solods (Whittig, 1959; Hallsworth and Waring, 1964; Zaidel'man et al., 2010; Sandoval and Reichman, 1971; Parakshin, 1984; Heck and Mermut, 1992).

The knowledge about clay mineral formation under salinization, solonization and solodization is scarce, controversial and generally based on qualitative (experimental) X-Ray Diffraction (XRD) data. Smectite, illite and/or kaolinite are the most common clay minerals described in the soils formed by these processes. In Sodic soils, Monteiro et al. (2012) suggested the neoformation of smectite trigged by ion accumulation in the footslope position of the profile. Antipov and Antipov (1995) and Chizhikova and Khitrov (2016) identified mainly illite in these soils, which were apparently inherited from the parent material. In Solodized Solonetzes, authigenic formation of smectite was indicated by Whittig (1959), Paquet et al. (1966), and Spiers et al. (1984), whereas in Solods, the formation of both kaolinite and illite is suggested, the former by Arshad and Pawluk (1966) and the later by Brunelle et al. (1976).

Mineral transformations through clay interstratification are scarcely described in salt-affected soils (e.g. Monteiro et al., 2012), although some mixed-layered minerals have been identified by their X-ray diffraction patterns, including illite-smectite, chlorite-smectite and chlorite-vermiculite (Whittig, 1959; Antipov and Antipov, 1995; Chizhikova and Khitrov, 2016). However, formation of mixed-layered phases as intermediate stages of mineral transformations should be highly expected in soils submitted to significant geochemical changes, such as those under solonization, solodization or weathering. Areas submitted to solodization, such as weathering zones, can experience significant leaching and acidification, triggering for example, the transformation of illite into smectite (Meunier, 2005; Galán and Ferrel, 2006). This process can generate illite-smectite (I-S) minerals, mainly through K^+ loss, the consequent opening of the interlayer and entrance of hydrated cations (Ca^{2+}, Mg^{2+} and others), and other minor rearrangement in the mineral's structure (Buey et al., 1998; Aldega et al., 2009).

Even more intense conditions of weathering and acidification may provoke smectite dissolution and possible complete precipitation of kaolinite (Karathanasis and Hajek, 1983; Ryan and Huertas, 2009) and/or its transformation into kaolinite through reactions that not involve the total rupture of the structure (Amouric and Olives, 1998). In the last case, progressive crystalochemical changes induce the formation of mixed-layered kaolinite-smectite (K-S), which implies in several structural transformations, including removal or inversion in the position of the smectite tetrahedral sheet, replacement of Mg/Fe by Al in the octahedral sheet and/or transformation of a smectite Al-rich interlayer into a kaolinite octahedral sheet (Karathanasis and Hajek, 1983; Amouric and Olives, 1998; Dudek et al., 2006; Ryan and Huertas, 2009).

In Nhecolândia (area of ~25,000 km^2), a sub-region of the Pantanal wetland, alkaline saline lakes have been transformed into brackish lakes due to the atypical entrance of freshwaters from the seasonal inundations (Almeida et al., 2003; Fernandes, 2007). This process has provided a gradual transformation in the soils, Saline-Sodic around the saline lakes and Sodic and degraded Sodic soils around the brackish lakes. The solonization and solodization processes are in total consonance with the geochemistry of the brackish lakes, inasmuch as Sodic soils dominate around the brackish lakes that have pH and EC more similar to those of saline water, whereas Solods dominate around the brackish lakes that present pH and EC more similar to the freshwaters (Furquim et al., 2017).

Because of these characteristics, the region offers a great opportunity to better understand mineral genesis during the evolution of salt-affected soils, which is still little documented in the international literature. Thus, the present research aimed to study the formation of clay minerals associated with a gradual transformation of Saline-Sodic to Sodic and Solod soils, assuming that the genesis of these minerals probably occurs through the generation of mixed-layer minerals, from the least to the most acidic environment.

2. Materials and methods

2.1. Environmental settings

The Pantanal wetland is a huge alluvial plain (area of 150,500 km^2) partially reached by seasonal inundation, located mainly in central-western Brazil and small portions of Bolivia and Paraguay (Fig. 1) (Padovani, 2010). The region is a modern sedimentary basin constituted mainly by fluvial sediments, which are currently deposited by the Paraguay River and its tributaries and distributary rivers (Silva, 1986; Assine, 2015). The altitudes range from 60 and 200 m, with slopes of less than 0.1% (Silva, 1986; Por, 1995). Due to its pristine ecosystems (Pott and Silva, 2016), part of the Pantanal is considered as Word Heritage Area by UNESCO.

The wetland is entirely in the Upper Paraguay River basin, which integrates the La Plata drainage basin, one of the biggest of the world (3.2 million km^2) (Carvalho, 1986; Collischonn et al., 2001). The climate is Tropical Savannah (Aw), according to Koppen classification (Por, 1995). The average temperatures varies between 22 and 26 °C, with October and December being the warmest months in the northern and southern latitudes, respectively, and July the coldest month in the whole region (Tarifa, 1986). The average annual precipitation ranges from 1100 to 1250 mm (Marengo et al., 2016). The rain is concentrated mainly from December to March, whereas the dry period occurs from June to August (Alfonsi and Camargo, 1986; Marcuzzo et al., 2010). An annual hydric deficit of at least 300 mm is registered in the Pantanal because of the high annual evapotranspiration rates (1400 mm) (Alfonsi and Camargo, 1986).

The Nhecolândia sub-region (area of 49,000 km^2), located in

[1] $NaX + H_2O \rightarrow HX + NaOH$, where X is the exchange complex (Fanning and Fanning, 1989; Bohn et al.,2001); $Na_2CO_3 \rightarrow 2Na + CO_3^{2-}$; $CO_3^{2-} + H_2O \rightarrow HCO^{3-} + OH^-$ (McBride, 1994).

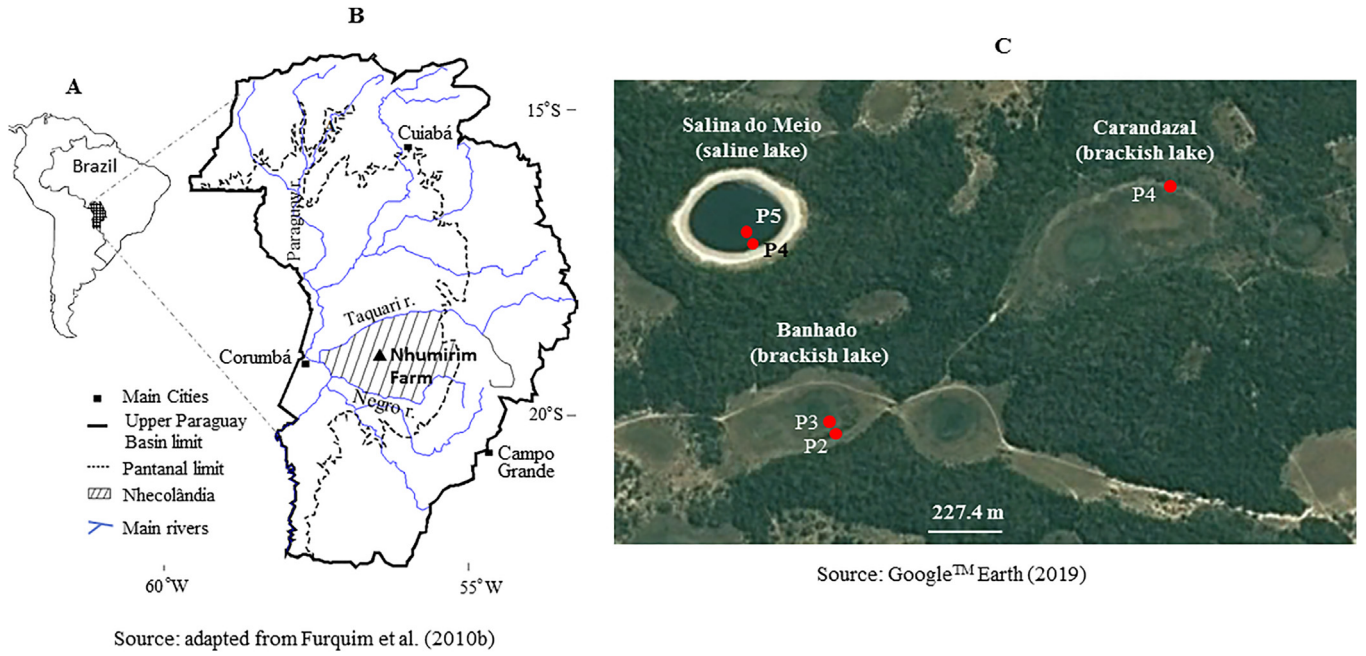

Fig. 1. A) Location of Brazilian Pantanal in South America; B) Location of Nhecolândia sub-region and Nhumirim Farm in the Brazilian Pantanal; C) Saline and brackish lakes of interest in this work and location of the studied pedons (P) (Nhumirim Farm); P4 and P5 around Salina do Meio were not under the lake during the soil survey because it was performed during the dry season.

central-southern Pantanal, corresponds to the southern half of the huge Taquari alluvial fan (Zani et al., 2012). The entire sub-region is covered by very similar sediments, composed mainly by whitish, fine to medium sands, which overlay reddish sands cemented by iron oxides (Assine and Soares, 2004). These whitish sands that occur near the surface are formed by quartz (Godoi Filho, 1986; Assine, 2003), with minor presence of feldspars such as microcline and albite (Furquim, 2007). The saline lakes occur only in this sub-region and are located on the top of sandy hills, which are the watershed of intermittent rivers. Due to higher topographical position of the sand hill/saline lake complex (3 to 5 m above the surroundings), these two geomorphological features are not typically reached by the seasonal freshwaters of the floods, allowing the development of forested savanna vegetation on the sand hills. Intermittent watercourses are formed by the coalescence of freshwater lakes during the seasonal inundation and are generally covered by open grass savanna or swampy grasslands during the dry season (Barbiero et al., 2002; Evans and Costa, 2013) The saline waters, mainly fed by rain precipitation (Freitas et al., 2019), are currently formed in the region by lake shrinkage due to the high evapotranspiration rates, producing waters with pH of 8.5 to 10.1 and EC from 6 to 68 dS m^{-1}. The freshwater from the floods, on the other hand, commonly presents lower pH $<$ 6.0 and EC $<$ 0.30 dS m^{-1} (Barbiero et al., 2002; Almeida et al., 2003).

The transformation of the saline lakes into brackish lakes, which present intermediate pH and EC between the fresh and saline waters, have occurred due to the erosion of the sand hills, the atypical input of freshwaters into the saline lakes and the formation of new intermittent watercourses by the coalescence of brackish lakes during the flood season (Almeida et al., 2003; Fernandes, 2007; Furquim et al., 2017). This process has been apparently active in the last 3000 years in the region (Furquim et al., 2017), confirmed by a set of evidence. In the aerial images, the preserved saline lakes are totally surrounded by forested savanna, whereas the brackish lakes are mainly surrounded by open grass savanna and/or grasslands, which typically occur in areas subjected to flood (Almeida et al., 2003; Fernandes, 2007; Evans and Costa, 2013). The aerial images also reveal that incipient watercourse channels link brackish lakes characterized by waters that are more similar to the saline lakes, whereas more developed channels link brackish lakes with waters that are more similar to the freshwaters (Almeida et al., 2003). The transformation of the Saline-Sodic soils, typically formed around the saline lakes, into Sodic soils and Solods around the brackish lakes is a direct consequence of these geomorphological and geochemical changes in the region (Furquim et al., 2017).

The Saline-Sodic soils occurring around the saline lakes are mainly comprised by a sequence of H-E-Bkg-Bnq horizons. The H is dark gray (10YR 4/1, dry), sand to loamy sand and prismatic and the E is light brownish gray (2.5Y 6/2, dry), sand and single grain. Below, the Bkg is gray (2.5Y 5/1, dry), sandy to loamy sand and massive, whereas the Bnq is an olive gray (5Y 5/2, dry) or gray (5Y 5/1 or 6/1, dry), sandy loam, massive and extremely hard due to the cementation of amorphous silica. The whole soil profiles have pH commonly higher than 10, EC higher than 9 dS m^{-1} and exchangeable sodium percentage (ESP) higher than 30% (Furquim, 2007; Furquim et al., 2008).

As briefly exposed in the Introduction, the Sodic and Solod soils occur around the brackish lakes with different characteristics. Considering the lakes studied by Furquim et al. (2017), the Sodic soils are more abundant around the Carandazal lake, whose waters present higher pH and EC (6.5 and 1.9 dSm^{-1}) and are relatively more similar to the saline waters. These Sodic soils are mostly composed by the horizons A, AB, Bnc1 and Bnc2. The A is dark grayish brown (10YR 4/2, dry) or grayish brown (10YR 5/2, dry), sandy, sandy loam or silt loam and mainly with platy structure, whereas the AB is gray (10YR 6/1, dry) or very pale brown (10YR 7/3, dry), sand to loamy sand and single grain. The Bnc1 and Bnc2 are olive (5Y 4/4, 5/3, dry) and olive (2.5Y 4/4, 5/3, dry) or olive brown (2.5Y 4/3; 4/2, dry), respectively, and both tend to be massive, sandy loam to sandy clay loam and extremely hard. The whole soil profiles tend to present EC smaller than 2 dS m^{-1} and the B horizons have pH $>$ 8 and ESP $>$ 15%, whereas the upper horizons generally present smaller values (Furquim et al., 2017).

The Solods are dominant around the Banhado lake, which has waters with the lowest pH and EC (6.2 and 0.8 dS m^{-1}) of the brackish lakes studied by Furquim et al. (2017), characteristics more similar to the freshwaters. These soils are most commonly formed by the horizons A, AB, Bc and Bnc2. The first two and the later horizons present morphological characteristics similar to the Sodic soils. The Bc is dark

yellowish brown (10YR 4/4, dry) or brown (10YR 4/3 or 5/3), sandy loam to clay loam, mostly massive and extremely hard. The whole Solod profiles present EC lower than 1 dS m^{-1} and ESP lower than 10%. The pH is acid to alkaline (5.0–8.0) in the B horizons and acid (4.9–5.8) in the upper horizons (Furquim et al., 2017).

The Bnc1, Bnc2 and Bc of the Sodic and Solod soils are genetically linked to the Saline-Sodic soils, representing a progressive transformation of the Bnq due to the freshwater entrance in the saline lake depression. The Bnc1 horizon is more similar to the Bnq, inasmuch as it presents an analogous subsurface position, greenish color, clay accumulation, significant hardness and relatively high pH and ESP. Bnc2 tend to present intermediate properties, whereas the Bc seems to present different characteristics from the Bnq, but it still maintains similar subsurface position, clayey texture and high hardness. Although Bc tend to have significantly lower pH and ESP than the other B horizons, it commonly presents an ESP higher than 5%, which corroborates its inheritance from the Saline-Sodic Soils (Furquim et al., 2017).

2.2. Studied samples

The soils located in the surroundings of saline and brackish lakes of Nhecolândia (Nhumirim Farm), were selected for this study based on the study of salt-affected soils by Furquim (2007) and Furquim et al. (2017) (Fig. 1). The studied soils comprise: i) two Saline – Sodic profiles (Typic Petraquepts) located around a saline lake, locally called Salina do Meio, which presents waters characterized by a pH of 9.6 and EC of 12.7 dS m^{-1} (Furquim, 2007; Furquim et al., 2010b); ii) one Sodic soil profile (Aquic Udorthents) located around the brackish lake called Carandazal, with waters presenting a pH of 6.5 and EC of 1.9 dS m^{-1}; and iii) one Sodic soil profile (Typic Udorthents) and one Solod profile (Aquic Udorthents), both located around the brackish lake called Banhado, which has waters characterized by a pH of 6.2 and EC of 0.8 dS m^{-1}.

The following eight samples, all from B horizons, were selected from these soils and investigated in the present study: a) Saline-Sodic soil (Salina do Meio lake): Pedon 4 (P4), horizon Bnq (80–100 cm); Pedon 5, horizon Bnq (90 + cm); b) Sodic soil (Carandazal lake): Pedon 4 (P4), horizons Bnc2 (60–77 cm), Bnc1 (77–98 cm) and Bnc2 (98–132 cm); c) Sodic soil (Banhado lake): Pedon 2 (P2), horizon Bnc1 (82–180 cm); and d) Solod (Banhado lake): Pedon 3 (P3), horizons Bc (130–185 cm) and Bnc2 (185–291 cm). These selected horizons show morphological and chemical characteristics that are representative of their progressive transformation due to the entrance if freshwater, as described in the Section 2.1 (Environmental Settings).

The soil survey occurred during the dry season (October), when the soils are at maximum exposition in the wetland. The description and sampling were performed in pits, where approximately 500 g of each horizon were collected. However, in Pedons 2 and 3 of the Banhado lake the survey below 180 cm was complemented with auger holes at the bottom of the trench. The location of each selected pedon in relation to the lake is shown in Fig. 1 and their geographical coordinates and main morphological, physical and chemical characteristics, published in other works, are summarized in Table 1. Further and more detailed characteristics about the studied soils can be found in Furquim (2007) and Furquim et al. (2017).

2.3. XRD analysis

The mineral composition of < 0.2 μm size fractions (fine clay), which represent approximately 60–70% to the total clay and contain most of the autochthonous minerals, was studied by XRD analysis, following the pre-treatments described in Jackson (1985). The samples were previously treated with sodium hypochlorite at 80 °C, buffered at pH 9.5, to remove organic matter (Anderson, 1963). The possible negative effects on the lattice of the clay minerals were disregarded, as attested by Dumon et al. (2014) in submicron clay fractions of soils. The samples were dispersed in mild alkaline solution (0.01 M Na_2CO_3, pH 8.6) and the clay fraction was separated from the silt by successive centrifugations at 600 rpm (75 *g*) for 5 min. The fine clay fraction (< 0.2 μm) was separated from the coarse clay fraction (2–0.2 μm) after successive centrifugations at 4000 rpm (3345*g*) for 20 min (40–100 times per sample). The fine clay fraction was saturated with K^+ and Mg^{2+}, by adding 1 M KCl and $MgCl_2$ solutions, further dialyzed in nanoporous membranes (MWCO 10,000) filled with ultrapure water, to remove the excess of chlorides. The samples were washed with water to remove excess chloride until a negative test with 1 M $AgNO_3$.

The saturated samples were studied in the XRD device as oriented mounts. Approximately 1 g of powdered samples was dispersed as suspensions in ultrapure water using an ultrasound probe. The suspensions were pipetted over a glass slide, dried at room temperature overnight (to achieve a minimal concentration of 10 mg cm^{-2}). The K-saturated samples were analyzed at room temperature and after heating at 550 °C for 2 h, in order to confirm the presence of kaolinite and the partial collapse of expansive clays. The Mg-saturated samples were studied in the air-dried state and as glycolated samples, after solvation with ethylene glycol (EG) at 60 °C, for 16 h. A Bruker D8 Advance XRD device was used, operating at 40 kV and 20 mA, with two Soller slits at 2.5° and divergence slit of 1.0 mm. All the samples were studied at the 3–35° 2θ scanning interval and 0.02° 2θ of step-size. The scanning speed was 1 s/step in K-saturated and air-dried Mg-saturated samples but it was increased to 5 s/step in the EG-solvated slides in order to improve the quality of the XRD patterns for computer modelling. The samples were also studied at the 59–64° 2θ interval as powder preparations, in order to study the octahedral occupancy of clay minerals present in the samples (060 peak series). The same XRD device was used, with similar instrumental settings, but at a very low scanning speed of 40 s/step, aiming to maximize the signal/noise ratio and improve the resolution of the 060 peaks.

2.4. Full XRD profile modelling

The full XRD profile modelling procedure was applied to the patterns of EG-solvated samples to investigate the existence of mixed-layered minerals (MLM) and provide quantitative information about clay minerals (Hubert et al., 2009, 2012; Dumon et al., 2014; Andrade et al., 2019). In the present study, the computer program NEWMOD 3.2.1 was used to simulate the experimental glycolated patterns. The experimental settings of the XRD device were introduced and several MLM and endmember minerals were tested until the calculated line reached a minimal residual difference in comparison to the experimental line. The following crystal-chemical parameters were considered for each mineral: the stacking order type for MLM (R parameter), octahedral Fe content (on $0_{10}[OH]_2$ basis for 2:1 layers and $O_5[OH]_4$ for 1:1 layers), K^+ content for illitic layers (on $O_{10}[OH]_2$ basis) and peak position. The peak width at half-maximum was best simulated by considering a normal distribution of crystallites parallel to 00 *l* planes, in the range represented by N min (smallest crystallites) and N max (biggest crystallites) for each mineral.

The total percentage of layers of illite, smectite, kaolinite and vermiculite in the phases of each sample was calculated according to the formula (Eq. (1)):

$$TL_x(\%) = \frac{\sum (BPx)(MLx)}{100\%} \quad (1)$$

where $TL_x(\%)$ is the total percentage of layers of each sample; x represents layers of illite, smectite, kaolinite or vermiculite; BPx is the final proportion of x-bearing phase in the sample (wt%); MLx is the proportion of the x layer in the MLM (wt%), considering the two mineral phases (as in Table 2).

Table 1
Selected morphological, chemical and particle size data of the soil profiles.

Soil profile	Color (dry)	Structure	Sand (0.05–2 mm)	Silt (0.05–0.002 mm)	Clay (< 0.002 mm)	pH-H_2O	EC	ESP
			g kg^{-1}				dS m^{-1}	%
Saline Sodic soils (Saline lake – Salina do Meio)								
Pedon 4 (P4) – 18°58′30″ S/56°38′48″ W								
H (0–5 cm)	10YR 4/1	Prismatic	946.1	17.8	36.0	10.32	30.32	> 30
E (15–55 cm)	2.5Y 6/2	Single grain	902.5	55.9	41.6	10.12	11.43	> 30
Bkg (55–80 cm)	2.5Y 5/1	Massive	882.2	67.9	49.9	10.80	13.30	> 30
Bnq (80–100 + cm)	**5Y 6/1**	**Massive**	**783.2**	**101.2**	**115.6**	**10.39**	**11.42**	**> 30**
Pedon 5 (P5) – 18°58′29″ S/56°38′49″ W								
H (0–5 cm)	10YR 4/1	Prismatic	822.7	91.8	85.4	10.22	43.01	> 35
E (20–40 cm)	2.5Y 6/2	Single grain	902.2	63.9	33.9	10.38	9.82	> 35
Bkg (40–90 cm)	2.5Y 5/1	Massive	802.8	121.9	75.3	10.81	13.93	> 35
Bnq (90 cm +)	**5Y 5/1**	**Massive**	**762.3**	**138.2**	**99.5**	**10.58**	**13.18**	**> 35**
Sodic soil (Brackish lake – Carandazal)								
Pedon 4 – (P4) – 18°58′23″ S/56°38′04″ W								
A2 (0–9 cm)	10YR 5/2	Platy	524.72	349.14	126.14	5.59	0.00	0.3
AB (9–34 cm)	10YR 6/1	Massive	794.11	180.91	24.99	6.27	0.19	3.2
Bw1 (34 – 60 cm)	10YR 7/1	Massive	677.95	246.87	75.19	6.38	0.35	2.5
Bnc2 (60–77 cm)	**2.5Y 4/4**	**Massive**	**455.34**	**269.45**	**275.21**	**8.38**	**4.20**	**15.5**
Bnc1 (77–98 cm)	**5Y 5/3**	**Massive**	**552.52**	**196.79**	**250.69**	**8.58**	**1.99**	**24.9**
Bnc2 (98–132 + cm)	**2.5Y 4/4**	**Massive**	**487.07**	**236.75**	**276.17**	**8.14**	**1.44**	**23.0**
Sodic soil (Brackish lake – Banhado)								
Pedon 2 (P2) – 18°58′49″ S/56°38′41″ W								
A1 (0–16 cm)	10YR 5/2	Single grain	959.10	26.22	14.68	5.04	0.19	2.9
AB (16–82 cm)	10YR 7/3	Single grain	972.21	16.78	11.01	5.06	0.05	9.7
Bnc1 (82–180 cm)	**5Y 4/4**	**Massive**	**706.86**	**77.42**	**215.73**	**8.70**	**0.70**	**34.0**
Bnc2 (180–240 cm)	2.5Y 5/3	–	790.92	60.11	148.97	8.96	1.30	21.3
Bnc1 (240–280 cm +)	5Y 4/4	–	785.36	59.77	154.88	8,87	0.80	21.5
Solod (Brackish lake – Banhado)								
Pedon 3 (P3) – 18°58′48″ S/56°38′42″ W								
A2 (0–13 cm)	10YR 4/2	Platy	834.04	92.90	73.07	5.19	0.35	0.6
AB (13–71 cm)	10YR 7/2	Massive	910.54	76.75	12.70	5.02	0.08	14.4
Bc ((88–115 cm)	10YR 5/6	Massive	396.19	277.83	325.98	5.42	0.38	6.6
Bw1 (115–130 cm)	10YR 7/2	Massive	728.09	116.46	155.45	5.59	0.18	5.5
Bc (130–185 cm)	**10YR 4/4**	**Massive**	**774.17**	**63.78**	**162.05**	**6.10**	**0.48**	**5.3**
Bnc2 (185–291 cm)	**2.5Y 4/4**	**–**	**749.87**	**58.00**	**192.13**	**7,70**	**0.87**	**2.4**
Bg1 (291–324 cm +)	10GY 4/5	–	854.07	62.25	83.68	8.04	–	5.7

Sources – Saline Sodic soils: Furquim et al (2007); Other soils: Furquim et al. (2017), Vidoca (2016), Santos (2016), Balbino (2017).
The horizons studied in the present work are bold.

2.5. STEM

The chemical composition and the distribution of the major elements in the individual mineral particles of the fine clay fraction was studied by Scanning Transmission Electron Microscopy (STEM) using a FEI Tecnai G^2 F20 instrument operated at 200 kV, equipped with a solid-state X-ray detector (HAADF – high angular annular dark filed). This system records images with different brightness intensities relative to the chemical composition of the analyzed materials, which is proportional to the atomic mass of the detected elements. This yields elemental maps, contrasting to the dark field of the images, useful to study the distribution of chemical elements in nanomaterials.

The samples were dispersed in ultrapure water and deposited onto a Cu grid coated with carbon film. From 5 to 11 individual crystals were analyzed in selected horizons from the three different soil systems studied. The crystals were scanned for approximately 30 min and the spatial distribution of the major structural elements present in the clay minerals (Si^{4+}, Al^{3+}, Fe, Mg^{2+} and K^{+}) was recorded. The Fe content was exclusively considered as Fe3+ because the X-ray detector does not differentiate the valence state of the element. The data were processed in the ES-Vision software, yielding maps with the elemental distribution for each major component of the clays.

2.6. Chemical composition of fine clay

The chemical composition of the selected samples of the fine fraction was studied by Inductively Coupled Plasma-Optical Emission Spectrometry (ICP-OES) after alkaline fusion. Approximately 100 mg of powder was fused in lithium metaborate and the resultant pellets dissolved in HCl (2%, v/v) + HNO_3 (4%, v/v) solution. The major elements (SiO_2, Al_2O_3, Fe_2O_3, CaO, MgO, K_2O, Na_2O and TiO_2) were determined by ICP-OES (Spectro Arcos) and the data normalized to 100%. The samples were analyzed in duplicates and the presented values are averages (wt%).

3. Results

3.1. XRD experimental results

The mineral assemblage of the coarse fractions (sand and silt fractions) in all soils were dominated by quartz, with minor amounts of microcline (K-feldspar group), probably in proportions less than 3% wt. (data not published). Mica minerals were not detected in the sand and silt fractions. The oriented XRD patterns of the coarse clay fraction (2–0.2 μm) present distinct basal peaks of kaolinite (~0.720 and 0.360 nm) and illite (~1.000, 0.500 and 0.333 nm) (Fig. S1A and B – Supplementary Electronic Material). No swelling clays were detected in these samples after glycolation, and no large asymmetries and peak displacements associated with the presence of MLM either. Quartz was identified in these samples (peaks at 0.426 and 0.334 nm) as well as traces of feldspars (peak at 0.324 nm). The X-ray scattering between 16 and 32 24°2θ, with no distinguishable maxima, may correspond to the

Table 2
XRD full profile fitting modelling parameters for the studied samples from the.

Sample	Minerals	% ML	$d_{001}A$	$d_{001}B$	Fe oct.			K ilt.	N max	N low	% final
					kaol	sm	ilt.				
Salina do Meio lake – Saline-sodic soil											
P4-Bnq	K-S	45–55	0.715	1.690	0.92	0.70	–	–	3	1	14
(80–100 cm)	K-I	99–1	0.718	0.998	0.70	–	0	0.80	34	16	6
	K-I	6–94	0.715	0.998	0	–	0.55	0.80	10	2	59
	I-S	84–16	0.998	1.690		0.98	1.04	0.84	3	1	21
P5-Bnq	K-S	58–42	0.715	1.690	0	0.75	–	–	4	1	9
(90 cm+)	K-I	98–2	0.718	0.998	0.85	–	0.95	0.8	42	26	5
	K-I	9–91	0.715	0.998	0	–	0.7	0.9	10	3	53
	I-S	81–19	0.998	1.690	–	0	0.9	0.8	5	1	34
Carandazal lake – Sodic soil											
P4-Bnc2	kaolinite	–	0.718	–	< 0.01	–	–	–	33	11	10
(60–77 cm)	K-S	90–10	0.718	1.690	0	0	–	–	10	2	5
	K-S	74–26	0.718	1.690	< 0.01	0	–	–	3	1	20
	K-I	11–89	0.720	1.010	0	–	0.72	0.80	13	3	45
	I-S	36–64	0.998	1.690	–	0.58	0.70	0.70	2	1	19
P4-Bnc1	kaolinite	–	0.715	–	0	–	–	–	34	19	13
(77–98 cm)	K-S	74–26	0.715	1.690	0	–			4	1	9
	I-S	91–9	0.998	1.690	–	–	0.75	0.80	14	5	58
	I-V	74–26	0.998	1.432	–	–		0.80	11	3	8
	I-V	74–26	0.998	1.432	–	–	0.30	0.55	3	1	12
P4-Bnc2	kaolinite	–	0.730	–	0	–	–	–	39	22	12
(98–132)	K-S	63–37	0.715	1.690	0	0.35	–	–	6	2	6
	K-I	11–89	0.715	1.000	0	–	0.60	0.80	14	5	45
	I-S	50–50	0.998	1.690	–	1.30	0.70	0.80	3	1	30
	I-V	80–20	0.998	1.432	–	–	0.60	0.80	8	2	7
Banhado lake Sodic soil											
P2-Bnc1	kaolinite	–	0.715	–	0.20	–	–	–	41	24	7
(82–180 cm)	K-S	92–8	0.715	1.690	0	1.30	–	–	25	12	5
	K-S	50–50	0.715	1.690	0	1.70	–	–	4	1	12
	K-I	8–92	0.715	0.998	0	–	0.95	0.70	13	4	26
	I-S	70–30	0.998	1.690	–	1.70	1.25	0.70	3	1	49
Solod											
P3-Bc	kaolinite	–	0.716	–	0	–	–	–	45	18	8
(130–185 cm)	K-S	96–4	0.715	1.690	0	1.00	–	–	18	7	6
	K-S	45–55	0.715	1.690	0	1.30	–	–	6	2	12
	K-I	9–91	0.715	1.000	0	–	1.00	0.80	17	6	25
	I-S	38–62	0.998	1.690	–	1.10	0.90	0.70	2	1	49
P3-Bnc2	kaolinite	–	0.715	–	0.01	–	–	–	61	33	11
(185–291 cm)	K-S	94–6	0.715	1.690	0	1.70	–	–	22	9	5
	K-S	94–6	0.715	1.690	0.20	–	–	–	8	3	6
	K-S	46–54	0.715	1.690	0	1.70	–	–	2	1	19
	K-I	5–95	0.715	0.998	0	–	0.60	0.80	19	9	20
	I-S	47–53	0.998	1.690	–	1.70	1.10	0.70	3	1	38

% ML – mixed-layering proportions, considering the two mineral phases; $d_{001}A$ and $d_{001}B$ – position, in nm, of the 001 peak of the first and second clay phase, respectively; Fe kaol, sm, ilt – octahedral Fe for kaolinite, smectite or illite layers, on a half unit cell basis ($O_{10}[OH_2]$ for 2:1 layers, $O_5[OH]_4$ for kaolinite layers); K^+ ilt – interlayered K^+ for illite layers, on $O_{10}(OH)_2$ basis; Nlow and Nmax – minimum and maximum number of layer per coherent scattering domain; % final – final proportion of each mineral phase in the assemblage.

presence of amorphous materials, very common in these soils (Furquim et al., 2008).. Traces of a feldspar group mineral were also detected in these samples (peak at 0.324 nm).

For the fine clay fraction, the experimental analysis of oriented XRD patterns indicates kaolinite, illite and smectite group minerals in all the studied samples, but with a varying contribution of each phase in the different XRD patterns (examples of each soil in Fig. 2). A trace of quartz (peak at 0.426 nm) was also detected in the Solod P3-Bnc2 sample (185–291 cm) from Banhado lake, likely inherited from the coarser fractions. The other samples do not present quartz peaks in the oriented patterns, although they were detected in the non-oriented patterns (Section 3.3). It suggests that small amounts of quartz may exist in these samples, but the quartz XRD peaks were likely masked by the peaks of oriented clay minerals.

Some characteristics were common to all samples. The existence of kaolinite was confirmed by the disappearance of 0.715 and 0.358 nm peaks after heating (550 °C) the K-saturated samples, caused by the dehydroxylation and subsequent destruction of its structure. Illitic minerals were identified by the sequence of peaks at 1.000, 0.500 and 0.334 nm, not affected by thermal treatments and EG solvation. A swelling 2:1 clay phase was identified after 001 peak shift from 1.400 nm Mg-saturated (air-dried samples) to 1.700 nm in EG solvated samples, in addition to the collapse of 1.200 nm peak to 1.001 nm after heating (550 °C) the K-saturated samples.

In the samples from the Saline-Sodic soils (P4 and P5 – Salina do Meio lake), there is a clear prevalence of illitic peaks, as previously verified by Furquim et al. (2010a,b). Kaolinite and smectite peaks are also present, but with lower intensity. In the Sodic and Solod soils of the Carandazal and Banhado lakes, the intensity of illitic peaks were considerably lower, while kaolinite and smectite basal peaks increased. The distinguishable peak maxima in the XRD patterns displays very small deviations from their original d-spacing values, which could be due to the irrational behavior of 00 *l* peaks, diagnostic for the identification of R0 MLM (Moore and Reynolds, 1997). This was more noticeable for the

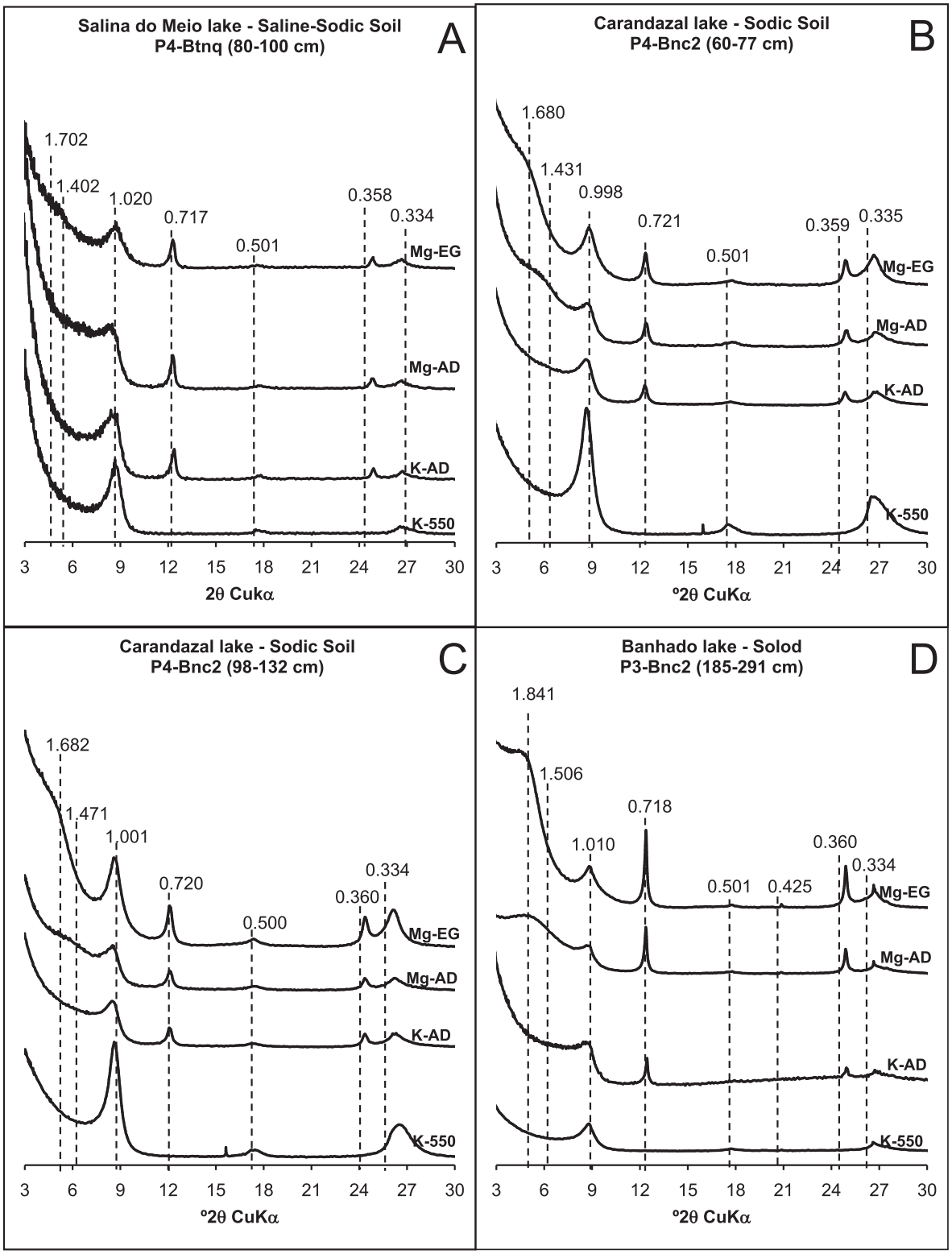

Fig. 2. Examples of the XRD patterns of the fine clay fraction (oriented mounts) for the sequence of treatments using K or Mg-saturation. The sequence includes: K-saturated samples analyzed at room temperature (K-AD) and after heating up to 550 °C (K-550); and Mg-saturated samples analyzed at air room temperature and after glycol solvation (Mg-EG). The peaks assigned in the figures are in nm and correspond to: 1.00–1.02 (0 0 1), 0.50 (0 0 2) and 0.33 nm (0 0 3) to basal peaks of illitic clay species in all treatments; 1.6–1.8 (001, expanded after EG), 1.4 (001 partially expanded in the MG-AD treatment), 1.0 (001, partially collapsed in the K-500 treatment) and 0.34–0.35 nm (0 0 5) to basal peaks of smectitic clay species; 0.71-0.72 (0 0 1) and 0.36 nm (0 0 2) of kaolinitic species in K-AD, Mg-AD and Mg-EG treatments, but totally collapsed in the K-550 treatment.

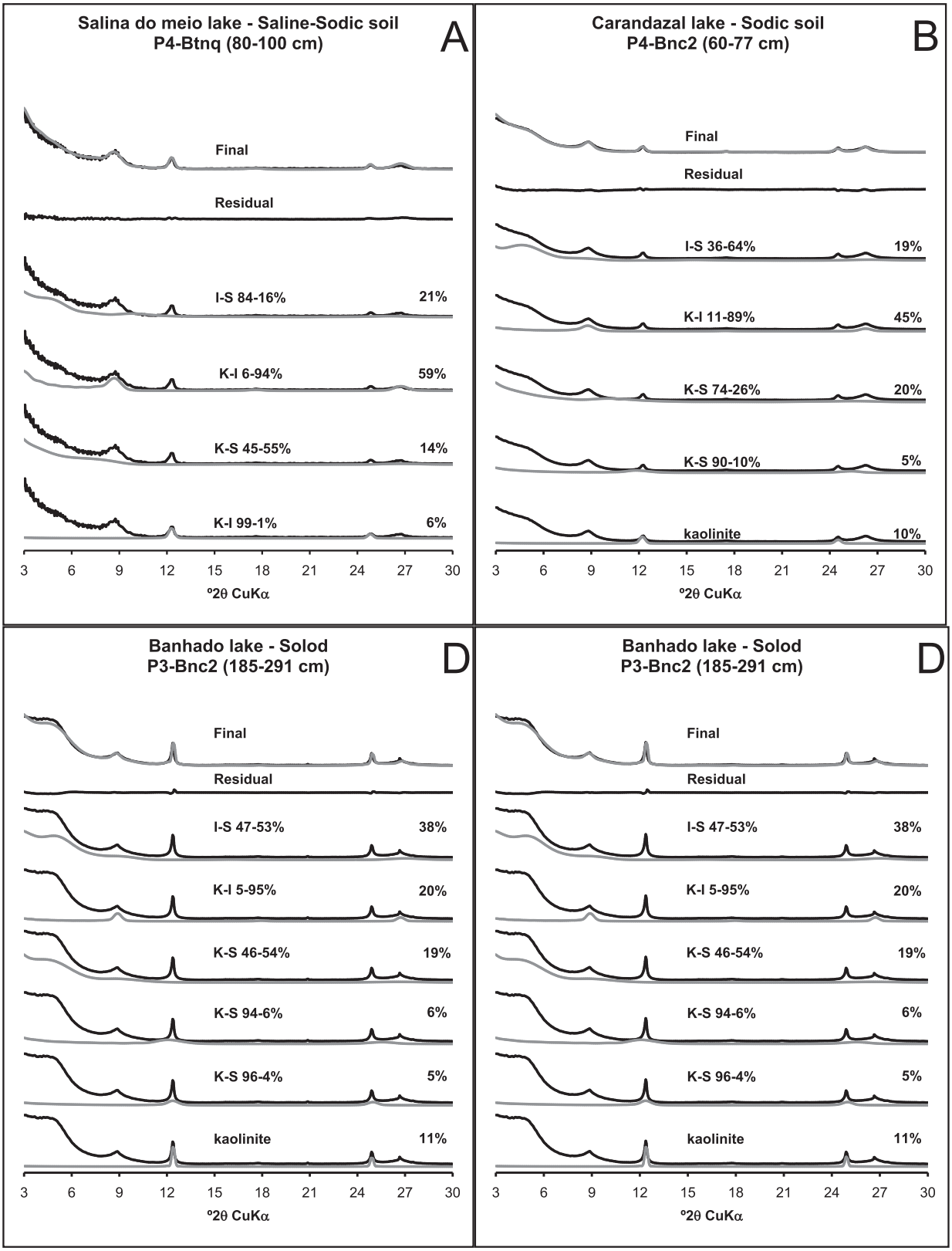

Fig. 3. Examples of XRD patterns calculated using NEWMOD 3.2.1 (gray lines), overlapped to experimental EG patterns (black lines). The calculated patterns are presented individually, together with their proportions in samples. On the top of the figures, the result of XRD full profile modelling (assigned as "Total") and the residual line, calculated from the difference between the experimental and calculated patterns. The parameters used to generate the calculated patterns are described in Table 3.

basal illite peak maxima (displacements of 0.1 and 0.2 nm in relation to illite endmember diagnostic d-spacing), but not observed in the kaolinite peaks, whose d-spacing were very close to the values described for the endmember phase (Brown and Brindley, 1980). Asymmetries and broad backgrounds adjacent to the most intense peaks were also present in all the XRD patterns, and these are other effects produced by the presence of R0 MLM (Moore and Reynolds, 1997), which were confirmed by the computational modeling procedure (Section 3.2). Most of these MLM did not yield distinguishable peak maxima because of their low proportions in the samples and/or low crystal ordering generated by mixed-layering (Table 2 and Fig. 3), but they are essential for producing the overall shape and intensity of XRD patterns.

3.2. Full XRD profile modelling

The experimental interpretation suggested the existence of MLM in the samples and the profile fitting modelling confirmed the existence of different types. The combination of layer types in the MLM used calculations considering the experimental identification that indicates illitic, smectitic and kaolinitic phases. The layer proportion in each MLM and its proportion in the samples was established after a trial and error procedure, until the experimental patterns fitted onto the experimental line. The STEM data supported the procedure (Section 3.5), confirming a chemical composition for individual crystals that matched the XRD modeling data. According to this procedure, the clay mineral assemblages were dominated by several MLM. A discrete kaolinite mineral and different R0 ordered MLM are present in the samples, including kaolinite-smectite (K-S), kaolinite-illite (K-I), illite-smectite (I-S) and illite-vermiculite (I-V), in a wide compositional range. The complete results are presented in Table 2 and examples of modelled XRD patterns are shown in Fig. 3.

In the two samples of the Saline-Sodic soil (P4 and P5), located around the lake with the highest water pH and EC (Salina do Meio) (Fig. 3A), the fine clay fraction presented K-I (91–94% of illite layers) and I-S (81–84% of illite layers) MLM as the major phases (Table 2). Both of them showed high Fe content in the illite, typical of glauconite or Fe-rich illite (Newman and Brown, 1987; Huggett and Cuadros, 2005), but the N min and N max values were moderate in K-I and low in I-S. Another two Fe-enriched MLM were detected in minor amounts: a K-S mineral, dominated by smectite layers in P4-Bnq and kaolinite layers in P5-Bnq, and a K-I with 98–99% of kaolinite layers, interpreted as a kaolinite endmember in the experimental patterns. The percentage of illite layers distributed in all the illite-bearing minerals (I-S and two K-I phases), calculated according to equation (1) (Section 2.4), was high in the two samples of the Saline-Sodic soil (Table 2, Fig. 4). The same calculation for total kaolinite and smectite layers corroborates their low percentages in this soil, confirming the dominance of illite in these samples.

The three samples (P4) from the Sodic soil of the Carandazal lake, intermediate water pH and EC values, presents less illite layers distributed in the different MLM (Fig. 3B, C, Table 2). Nevertheless, such as in the Saline-Sodic soil, Fe-enriched K-I and/or I-S minerals with ~90% of illite layers and moderate N max and N min values still dominated the samples. Fe-enriched I-S with low N max and N min values, dominated by smectite (64% of the layers) in the P4-Bnc2 (60–77 cm) and with intermediary proportions of illite and smectite (50% for each layer type) in the P4-Bnc2 (98–132 cm), arises in this soil (Fig. 4). Another four minerals were detected in minor amounts: a K-S with 63–74% of kaolinite layers, a K-S with 90% of kaolinite layers, a kaolinite endmember, and an illitic I-V mineral, with 74–80% of illite layers.

In the Sodic soils, the percentage of illite decreases (in K-I, I-S and I-V) while kaolinite (in discrete kaolinite, K-S and K-I), smectite (in K-S and I-S) and vermiculite (in I-V) layers of all minerals increase in comparison with Saline–Sodic soil (Table 2, Fig. 4). It is important to highlight that the highest percentages of illite and the lowest percentages of kaolinite and smectite layers in the Sodic soil were in the Bnc1 horizon, which presents the highest similarities with the greenish and near-impervious Bnq horizon of the Saline –Sodic soil.

Around Banhado lake, which has the lowest water pH and EC values, samples from a Sodic (P2) and a Solod (P3) soil were studied. In the Sodic soil (P2), such as that described around Carandazal lake, Fe-enriched and illitic I-S and K-I were the dominant minerals (Table 2). The I-S with low N max and N min values presented a lower amount of

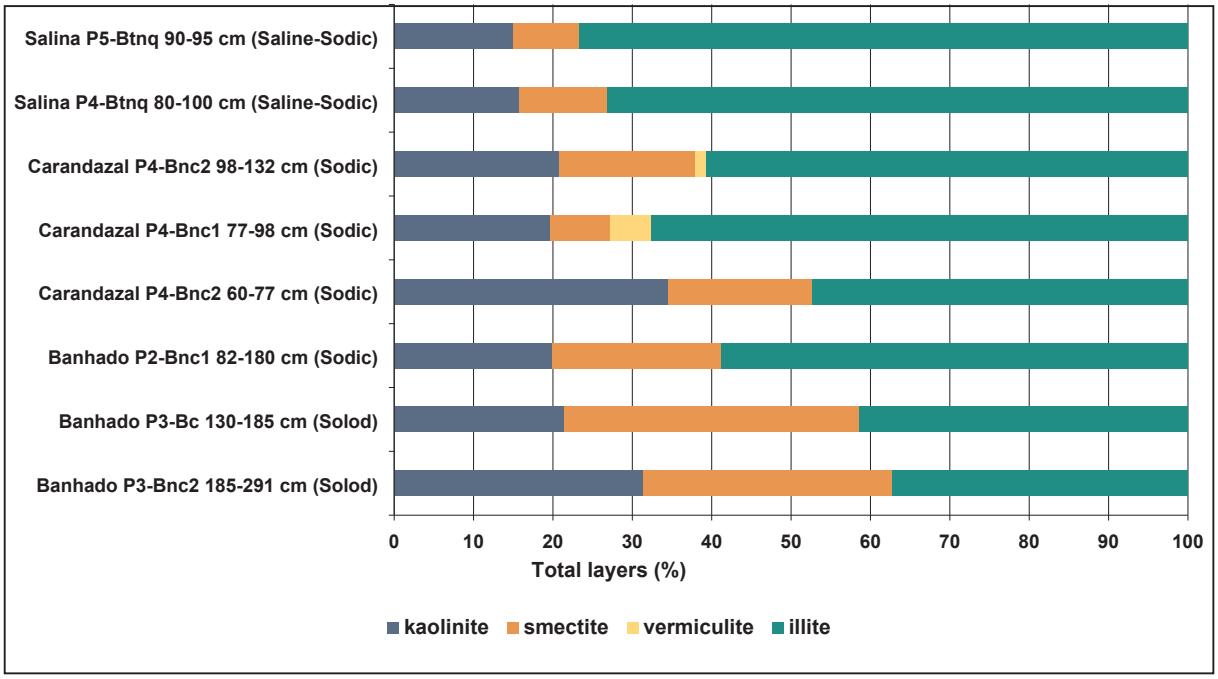

Fig. 4. Distribution of the four different types of clays used in the XRD full profile modelling, performed with NEWMOD 3.2.1, for all the studied samples (fine clay fraction). These proportions correspond to the values calculated using Eq. (1), according to the layer type proportions each MLM and their % wt. in the samples (Table 2).

Table 3
Chemical composition (ICP-OES) of the fine clay fraction, for the major elements. Minor and trace elements are not presented.

	Depth cm	SiO_2 wt%	Al_2O_3	Fe_2O_3	MgO	K_2O	CaO	Na_2O	MnO	TiO_2
Salina do Meio lake – Saline-Sodic soil										
P4-Bnq	80–100	54.9	14.7	9.0	2.6	4.1	0.2	0.3	0.7	0.7
P5-Bnq	90 +	55.5	14.1	10.0	2.8	4.7	0.2	0.4	0.6	0.6
Carandazal lake – Sodic Soil										
P4-Bnc2	60–77	55.4	11.3	11.1	1.8	0.4	0.0	1.0	0.3	0.3
P4-Bnc1	77–98	54.3	11.8	11.1	2.1	0.2	0.0	0.7	0.2	0.3
P4-Bnc2	98–132	54.8	11.1	12.0	2.0	0.6	0.1	0.9	0.3	0.2
Banhado lake Sodic Soil										
P2-Bnc1	82–180	56.1	12.0	11.0	1.7	0.1	0.5	0.3	0.4	0.2
Solod										
P3-Bnc2	130–185	57.0	12.2	10.5	1.6	0.1	0.6	0.3	0.4	0.3
P3-Bc	185–291	53.1	11.9	11.2	1.5	0.1	0.1	0.4	0.3	0.3

illite in the crystals (70% of illite layers) than in the Sodic soil around the Carandazal lake, whereas K-I, with intermediate N max and N min values, was similar to the Carandazal lake soil, presenting 92% of illite in the crystals. Three other minerals were identified in minor amounts in the sample: a kaolinite endmember, a K-S enriched in kaolinite (92% of kaolinite layers), and a K-S with similar proportions of kaolinite and smectite layers (50% of each). This soil presented percentages of illite (in K-I and I-S), kaolinite (in discrete kaolinite, K-S and K-I) and smectite layers (K-S and I-S) that were similar to the Sodic soil of the Carandazal lake (Table 2, Fig. 4).

The Solod soil occurring around the Banhado lake showed an important reduction in the proportion of illitic MLM and an increase in the proportions of MLM rich in smectite layers (Fig. 3D and Table 2). The two samples (P3) displayed a dominance of Fe-rich I-S (53–62% of smectite layers, with low N max and N low values) and Fe-rich K-I (91–95% of illite layers) with intermediate N max and N min values. Four other minerals were identified in minor amounts in the samples: a K-S slightly dominated by smectite layers (54–55% of smectite layers), a kaolinite endmember, and two K-S minerals, with 94–96% of kaolinite layers, one Fe-enriched and other Fe-depleted.

The percentage of illite (K-I and I-S), kaolinite (in discrete kaolinite, K-S and K-I) and smectite layers (in K-S and I-S) is more evenly distributed in the Solod samples (Table 3, Fig. 4). This corroborates with the significant decrease of illite and the concomitant increase of smectite in the samples, in comparison with the other studied soils. The percentages of kaolinite layers are similar to that in the Sodic soils, but the number of kaolinite-bearing phases (especially K-S) is higher in the Solod. It is important to highlight that the lowest percentages of illite and the highest percentages of smectite layers of the Solod are in the Bc horizon, which presents different morphological and chemical characteristics from the greenish and near-impervious Bnq horizon of the Saline–Sodic soil.

3.3. Octahedral occupancy (060 XRD peaks)

The XRD patterns of the 060 region show the prevalence of dioctahedral occupancy in all the samples, with two remarkable visible peak maxima at 0.151 and 0.149 nm (Fig. 5). These two peaks correspond to the dioctahedral sites of 2:1 Fe-rich (Deocampo et al., 2009) and to kaolinite layers (Brindley and Brown, 1980), respectively. Between these two peak maxima, there is a region that may be associated with Al-rich dioctahedral sites of 2:1 layers, at 0.150 nm (Brindley and Brown, 1980). A peak maxima at 0.154 nm with varying intensities could be observed in all the samples, attributed to the diffraction of quartz (Fanning and Fanning, 1989).

The 2:1 Fe-rich dioctahedral intensity was higher than that of kaolinite in all the samples. This result is consistent with the XRD full profile modelling results, which showed a high number of MLM with 2:1 layers. More details about the 060 region of the Saline-Sodic soil from the Salina do Meio can be found in Furquim (2007), but the peak maxima at 0.151 nm was remarkably dominant, corroborating the strong presence of Fe-illite and glauconite. The Sodic soils from the Carandazal and Banhado lakes presented this 2:1 maxima more distinguishable than the kaolinite peak, which seems to merge into a broad asymmetry towards higher 2θ angles, commonly observed in K-S phases (Dudek et al., 2006). In the Solod soil from the Banhado lake, however, the kaolinite maxima was more visible, although with an apparent lower intensity than that of the Fe-rich 2:1 clays.

3.4. Bulk chemical composition of the fine clay fraction

The bulk chemical composition of samples is presented in Table 3. The samples contain SiO_2, Al_2O_3 and Fe_2O_3 as the major elements (comprising ~76–80% of the sample mass), with minor amounts of K_2O, MgO, MnO, TiO_2, Na_2O and CaO. These elements are the structural components of the dioctahedral clay minerals detected in the samples (Newman and Brown, 1987) and the proportions among them corroborate the dominance of Fe-enriched phyllosilicates pointed by the XRD modelling. The SiO_2 (tetrahedral position) and the Fe_2O_3 (octahedral position) remained relatively constant in all the samples, whereas the Al_2O_3 (tetrahedral and octahedral position) and MgO (octahedral and/or interlayer positions) are slightly higher in the Saline-Sodic soil (Salina do Meio lake).

A noticeable difference was observed for K_2O content, which was very high for the two samples from the Saline-Sodic soil (P4-Bnq and P5-Bnq) when compared to the others. These values are certainly associated with the high amounts of illite-rich MLM in these samples (Table 2). The Na_2O values were surprisingly higher in the Sodic soil from Carandazal lake. Higher values were expected in the Saline-Sodic soils occurring around the Salina do Meio lake, where the water pH and EC are substantially higher (Furquim et al., 2010b).

3.5. STEM

Only few crystals in the samples were free of contamination or from the overlapping effect with other crystals to be analyzed as single mineral particles, but they were considered representative of the phases detected by XRD (Table 2). In the selected samples from the three different lakes, four compositional types were detected. Crystals with a hexagonal-like shape (and rounded edges) and kaolinite-like composition were chemically mapped (assigned as K, Table 4), characterized by high Al, low Fe and very few or null content of alkali cations (example in Fig. 6A). They represent the kaolinite endmember phase (or K-S very rich in kaolinite layers) identified by XRD.

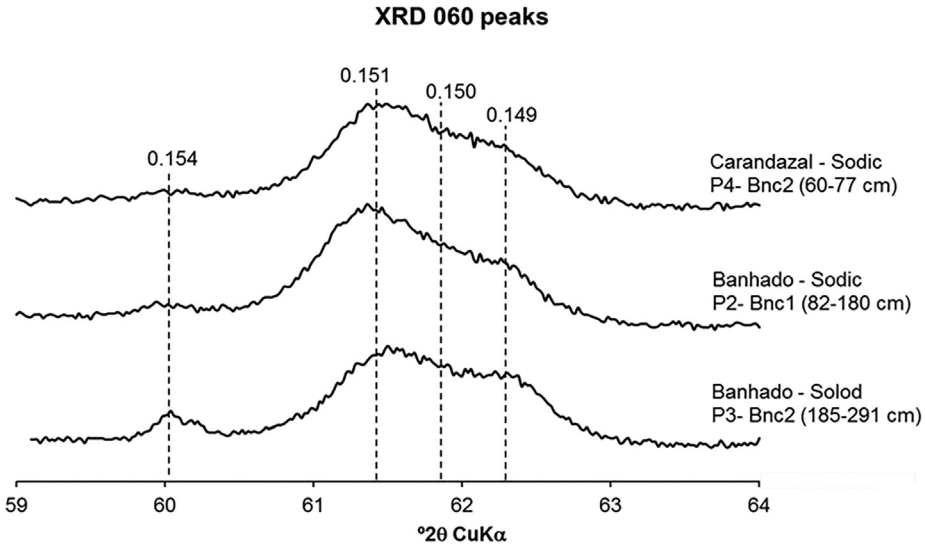

Fig. 5. Examples of XRD patterns in the region of 060 peaks, related to octahedral occupancies in the clay minerals. The peaks assigned in the figures are in nm and correspond to Al-rich dioctahedral occupancy in 1:1 layers (0.149 nm), Al-rich dioctahedral occupancy in 2:1 layers (0.150 nm) and Fe-rich dioctahedral occupancy in 2:1 layers (0.151 nm). The peak at 0.154 refers to remnant quartz in samples.

Table 4
Normalized chemical composition (wt., %) of individual clay crystals analyzed by STEM in selected samples. The notation used for each crystal represents kaolinitic (K), illitic (I), kaolinite-smectite (K-S) or illite–smectite (I-S) compositions. Only the main structural cations are presented.

	SiO_2	Al_2O_3	Fe_2O_3	MgO	K_2O
	% wt.				
Carandazal lake – Sodic soil					
P4-Bnc2 (60–77 cm)					
2 (I)	68.0	6.3	17.1	1.6	6.9
4 (K-S)	58.0	37.8	1.5	2.5	0.3
P4 – Bnc1 (77–98 cm)					
5 (K)	68.2	29.7	1.7	0.0	0.5
14 (K)	55.4	44.0	0.6	0.0	0.0
Banhado lake – Sodic soil					
P2-Bnc1 (82–180 cm)					
3 (K-S)	63.6	28.4	2.7	4.9	0.0
13 (I-S)	65.6	17.2	6.3	3.0	3.5
15 (I-S)	66.7	9.9	11.3	9.4	2.7
Banhado lake – Solod					
P3-Bnc2 (130–185 cm)					
5 (K-S)	65.5	14.2	13.7	6.6	0.0
7 (K)	53.7	44.0	2.3	0.0	0.0

The second and third types include particles with high SiO_2/Al_2O_3 ratios, moderate Fe_2O_3 and minor amounts of MgO or K_2O, representing the MLM rich in smectite layers. They were assigned as I-S when K^+ content was moderate (effect of illite layers) or K-S, when Mg^{2+} content was higher (minor or null effect of illite layers) and a moderately high Al^{3+} content (likely presence of kaolinite layers) (example in Fig. 6B). These crystals have a sub-rounded hexagonal shape (which can be associated with the prevalence of kaolinite layers) or anhedral shapes.

The fourth type (assigned as I in Table 3) is represented by only one example (Fig. 6C), in sample P4 Bnc2 (60–77 cm) of Sodic soil (Carandazal lake), related to an illitic composition. This crystal shows high Fe, Mg^{2+} and K^+, very similar to the glauconite crystals described in Salina do Meio (Furquim et al., 2010a) and other hypersaline environments (Huggett and Cuadros, 2010; Andrade et al., 2018). This composition matches the Fe-rich illite endmember/glauconite or MLM rich in these layers, such as K-I or I-S (~90% of illite layers) (Table 2). Other crystals with similar compositions were detected in samples from the three lakes, but the excess of Si^{4+} and other structural elements hampered the accuracy of identification.

The chemical mapping provided by STEM showed different patterns of elemental distribution in the crystals. The major elements Si^{4+} and Al^{3+} were ubiquitous and evenly distributed in the four compositional types. The distribution patterns of Fe varies: in kaolinitic crystals, the element is randomly distributed and rare (Fig. 6A), but becomes less uneven in the crystals with prevalence of 2:1 layers, where Fe content increases (Fig. 6B). Crystals with smectitic composition exhibit Mg^{2+} equally distributed along the analyzed surfaces, with a few patches where the element is not detected. K^+ distribution, however, is random in smectitic crystals with low amounts of the element (1–2%) (Fig. 6B). In the illitic crystal (Fig. 6C), it follows the spatial distribution observed for the major elements, occupying the majority of analyzed areas.

4. Discussion

The structural and chemical characterization of the fine clay fraction suggest a sequential transformation in the mineral assemblage, consistent with the changes in the morphological and chemical properties driven by solonization and solodization that take place in the Sodic and Solod soils around Carandazal and Banhado lakes (Furquim et al., 2017). These soils show a progressive loss of alkalinity and salinity that results in cation leaching and acidification, triggering the mineral transformations described below and summarized in Fig. 7.

In the B natric horizons from the Saline-Sodic soils (P4-Bnq and P5-Bnq), the Fe-illitic phases prevail, mainly as K-I and I-S MLM (Table 2, Fig. 4). This result is in agreement with the clear dominance of Fe-illite/glauconite, both interstratified mainly with smectite, observed by Furquim et al. (2010a) in the same samples. These authors showed that the Fe-enriched mica is formed by direct precipitation from the soil solution, aided by the suitability of the geochemistry if the local subsurface and surface water for this process, such as high pH, negative Eh and appropriate $Si(OH)_4$, K^+, Mg^{2+} and Fe concentrations (Harder, 1974, 1980; Barbiero et al., 2008).

Kaolinite-rich MLM (K-I, 98–99% of kaolinite) and kaolinite endmember were assumed as detrital in the samples. The geochemical conditions in the Saline-Sodic soils are very different from those ideal for kaolinite formation, i.e. low pH, low soluble K^+ and good drainage conditions (Tardy et al., 1973; Bohn et al., 2001; Velde, 1995). In addition, the area that is the source of sediments and water for Nhecolândia (Maracaju Plateaux) is covered by highly weathered soils where Fe-rich kaolinite prevails (Gardi and Angelini, 2014), which are further deposited in Nhecolândia. In the soils more affected by acidified waters (Solod Soils), the kaolinization reaction probably leads to the formation of endmember kaolinite, but it is impossible to separate its contribution from the minerals inherited from the forementioned source areas.

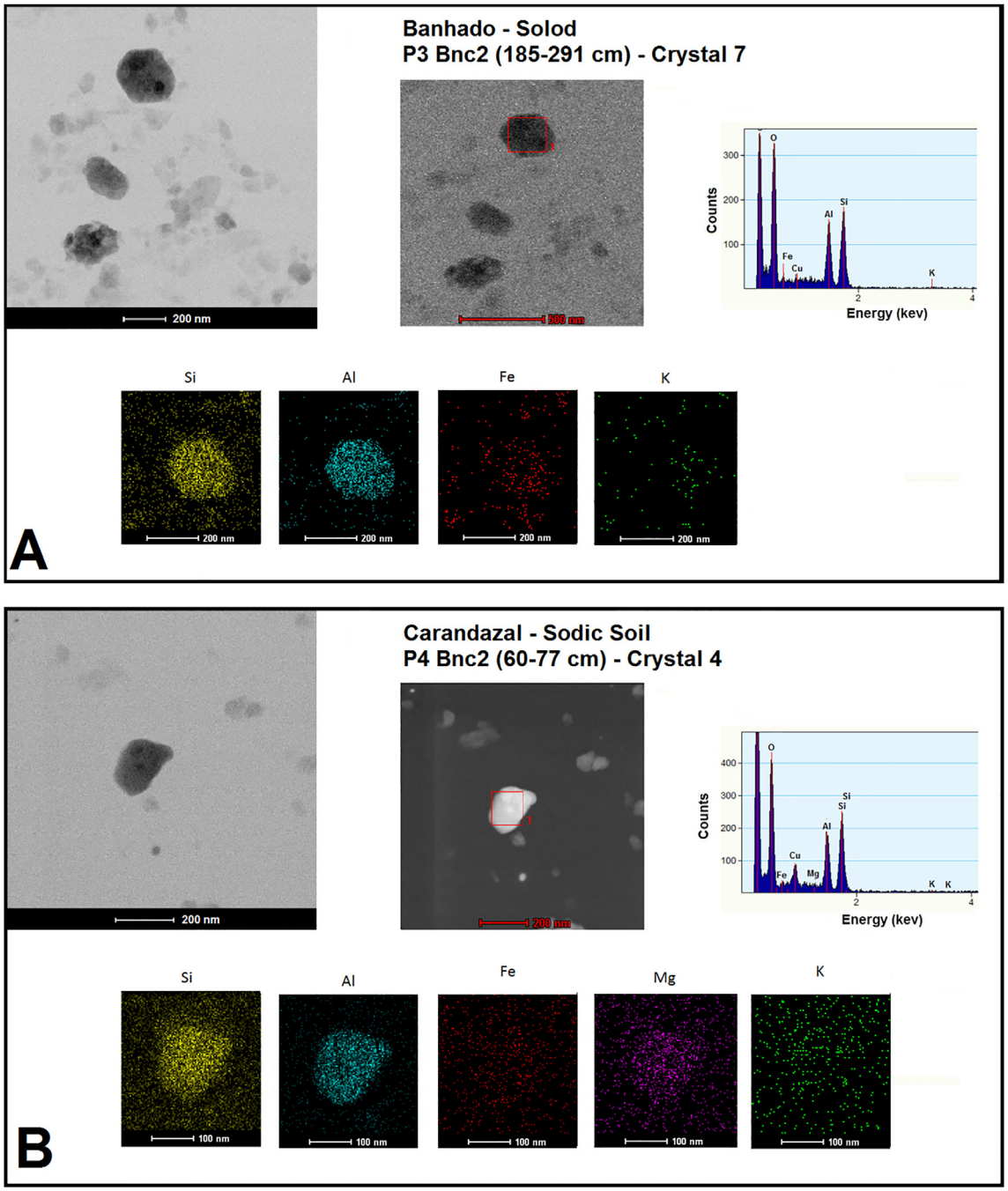

Fig. 6. STEM images, EDS spectra and STEM elemental mapping for the four representative composition types detected in the samples: A – kaolinitic composition, B – smectite-rich K-S composition, C – illitic composition.

Several of the MLM detected in the systems affected by brackish water, in different compositional ranges, are associated with the water geochemical changes from Saline-Sodic to Sodic and Solods soils (Fig. 7). The illite-rich MLM (K-I and I-S) are still common and quantitatively dominant in the Sodic soils associated with Carandazal (P4) and Banhado lakes, but it is important to highlight that in Banhado lake, unlike the Solods, the freshwater input reaches the Sodic soil at a lower frequency because of its high topographical position (Furquim et al., 2017). Although illitic minerals are prevalent in these samples, the total illite content is lower in comparison with the Saline-Sodic soils (Fig. 4). On the other hand, the percentage of smectite and kaolinite layers is clearly higher within the mineral phases, distributed in K-S and I-S (Table 2, Fig. 4). The existence of I-V and I-S in these samples can be interpreted as the first stage of Fe-illite transformation due to water acidification. In the Saline-Sodic soils, I-S is mainly composed by illite layers while in the Sodic soils (Carandazal lake, samples P4-Bnc2 98–132 cm and P4-Bnc1 77–98 cm), I-S contains more smectite layers and I-V is present in lower proportions. This pattern of MLM formation is in agreement with models of Fe-illite/glauconite weathering in alkaline soils (Skiba et al., 2014; Kiesel et al., 2018; Skoneczna et al., 2019).

In the Solod soil, associated with Banhado lake (P3), the solodization imposed more intense mineral transformations. The K-I and I-S MLM are still the dominant phases, but differently from the other soils, the latter phase is in higher proportions and is no longer dominated by illite layers, consistent with the lower total illite contents in these samples (Fig. 4). The percentage of kaolinite layers remained within the same range as the Sodic soils, but the number of kaolinite phases

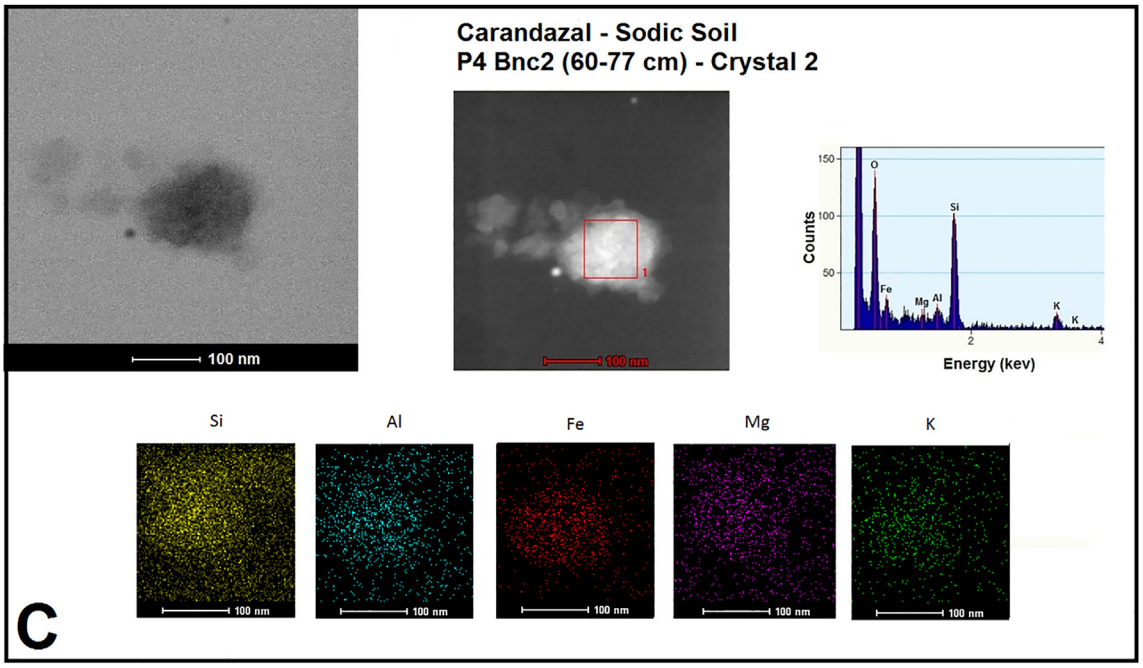

Fig. 6. (*continued*)

increased, especially K-S, which is probably responsible for a more visible kaolinite 060 peak in the Solod samples (Fig. 5).

These trends can also be observed along the Bnc1, Bnc2 and Bc horizons, which represent the progressive morphological and chemical transformations in the Bnq of the Saline-Sodic soil (Section 2.1). Thus, in the Sodic soil (P4, Carandazal lake), the highest percentages of illite and the lowest percentages of kaolinite and smectite layers are in the Bnc1 horizon, which is the first stage of transformation of the Bnq, typically formed under the alkaline conditions of the saline lake. In the Solod (P3, Banhado lake), the lowest percentages of illite and the highest percentages of smectite layers are in the Bc horizon, which is the last stage of transformation of the Bqn (Furquim et al., 2017).

The wide compositional range of kaolinite-bearing MLM (K-S and K-I) in the samples fits into reactional models that describe the transformation of 2:1 into 1:1 layers without the complete dissolution of 2:1 layers and the reprecipitation of the less soluble products. These models address the partial maintenance of original 2:1 layers as evidence of the progressive transformation, without the complete disruption of the crystal structure. The reactional steps include the strip of tetrahedra, proton attachment in the apical oxygen of the remaining octahedral sites, partial collapse to a ~0.7 nm d-spacing, reduction of layer charge by isomorphic substitutions of Mg/Fe by Al and Al by Si in the octahedral and tetrahedral sheet, respectively, tetrahedral inversion and the removal of interlayer cations (Amouric and Olives, 1998; Dudek et al.,

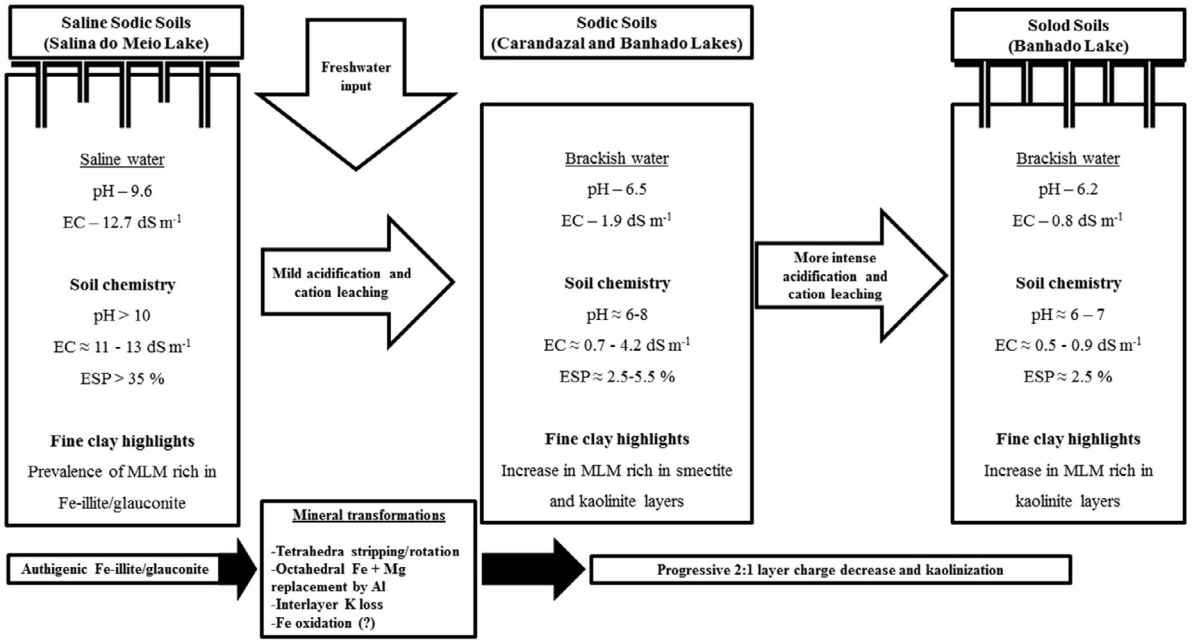

Fig. 7. Graphic scheme that summarizes the geochemical and mineral transformations in the soils around the three different studied lakes. The chemical and mineral information contained in the boxes are only the main chemical and mineral features of the three soil types. The complete information and mechanisms can be checked in Tables 1 and 2, and through the Section 4 (EC – electric conductivity, ESP – exchangeable sodium percentage).

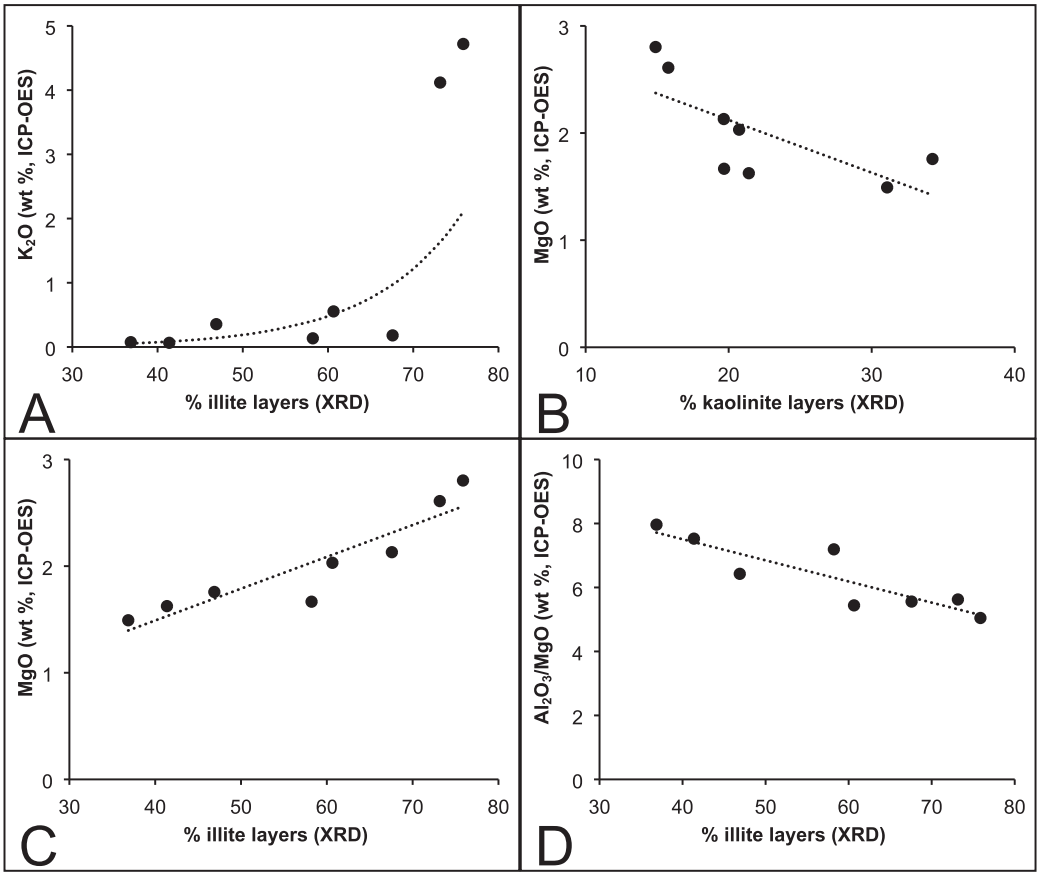

Fig. 8. Correlations between total clay type layers (calculated from XRD data) and the bulk chemical composition (ICP-OES data) of the samples.

2006; Ryan and Huertas, 2009). This model matches with transformation of mica group minerals into kaolinite via MLM (Dong et al., 1998; Andrade et al., 2019), and smectite to kaolinite transition under high weathering conditions (Ryan and Huertas, 2009; Pincus et al., 2017; Oliveira Junior et al., 2019).

The kaolinization of 2:1 clays is not restricted to the most leached soils. The K-S and K-I phases were detected in samples where alkalinity and salinity remain relatively high (e.g., P4-Carandazal, Table 2). However, the high proportion and the wide compositional range of K-S minerals described for Solods indicate that the kaolinization of smectite layers is more advanced in these samples, consistent with the high degree of solodization described by Furquim et al. (2017). The kaolinite endmember detected in lower amounts in Solods, but with a higher N max and N min values, represents the final product of this process as solodization advances.

The structural changes mentioned above are supported by the chemical characterization. The most significant variation in the bulk chemical composition is related to K_2O content (Table 3, ICP-OES results), which is higher in the Saline-Sodic soils and correlates with the total amount of illite layers, as expected (Fig. 8A). In the ternary plot containing Al_2O_3-Fe_2O_3-K_2O normalized contents (ICP-OES data), the association of Saline-Sodic samples with K_2O is very clear (Fig. 9A, green circle). These samples are represented by distinct points in the plot due to their high K_2O content, while the other samples (Sodics and Solod, blue circle) present lower K_2O values and are dominated by Fe_2O_3 and Al_2O_3, as the illitic MLM become less common (Table 2, Fig. 9A). The arrow in Fig. 8A indicates the direction of chemical transformation as the samples undergo the progressive acidification, and the number of MLM rich in smectite and kaolinite layers increases.

The STEM data show that K^+ is sparsely distributed in the smectized and kaolinized crystals from the Sodic and Solod soils (Fig. 6A and 6B), concentrated in some patches where the layer charge probably remains high. In the only crystal assigned as "illitic" (Sodic soil, P4-Carandazal lake), however, K^+ is well distributed due to the high layer charge along the crystal (Fig. 6C). This information suggests that K^+ is rapidly depleted from the interlayer spaces when illite undergoes alteration, as a result of layer charge reduction. In the ternary plot containing Al_2O_3-Fe_2O_3-K_2O normalized STEM data (Fig. 10A), it is possible to visualize the progressive depletion of K: the only illitic crystal (green circle) is distinct from the crystals with smectitic (orange circle) and kaolinitic compositions (blue circle) on the basis of K and Fe, which decrease as they assume a kaolinitic composition (represented by the arrow in Fig. 9A).

The MgO values (ICP-OES, Table 3) are negatively related to kaolinite layers (Fig. 8B) because the kaolinization of 2:1 layers in the Sodic and Solod soils includes Mg^{2+} loss (Dudek et al., 2006; Ryan and Huertas, 2009). This effect is also evident by the negative correlation between Al_2O_3/MgO and % of illite layers (Fig. 8D), enhancing the relationship between aluminization and the decrease of illite layers in the samples. Conversely, a positive correlation is observed for illite layers, with higher MgO in the Saline-Sodic samples (Fig. 8C). It matches the chemical composition attributed to Fe-enriched illite layers (Fe-illite and glauconite-like composition), since this mineral also contains Mg^{2+} (in addition to Fe) as octahedral cation (Odom, 1984; Furquim et al., 2010a; Huggett and Cuadros, 2010). In the ternary plot containing Al_2O_3-Fe_2O_3-MgO values (Fig. 9B), the association of MgO with illitic composition is clear (samples within the green circle): the two Saline-Sodic samples are distinct points in the plot, with Mg partially replacing octahedral Fe. The other samples are very similar to each other (within the blue circle), with Al and Fe prevailing as octahedral cations due to acidification and leaching.

The STEM data show Mg^{2+} is well distributed in I-S and K-S crystals, even more so than Fe (Fig. 6B). This element can be common in both octahedral and interlayer sites, not being restricted to the latter

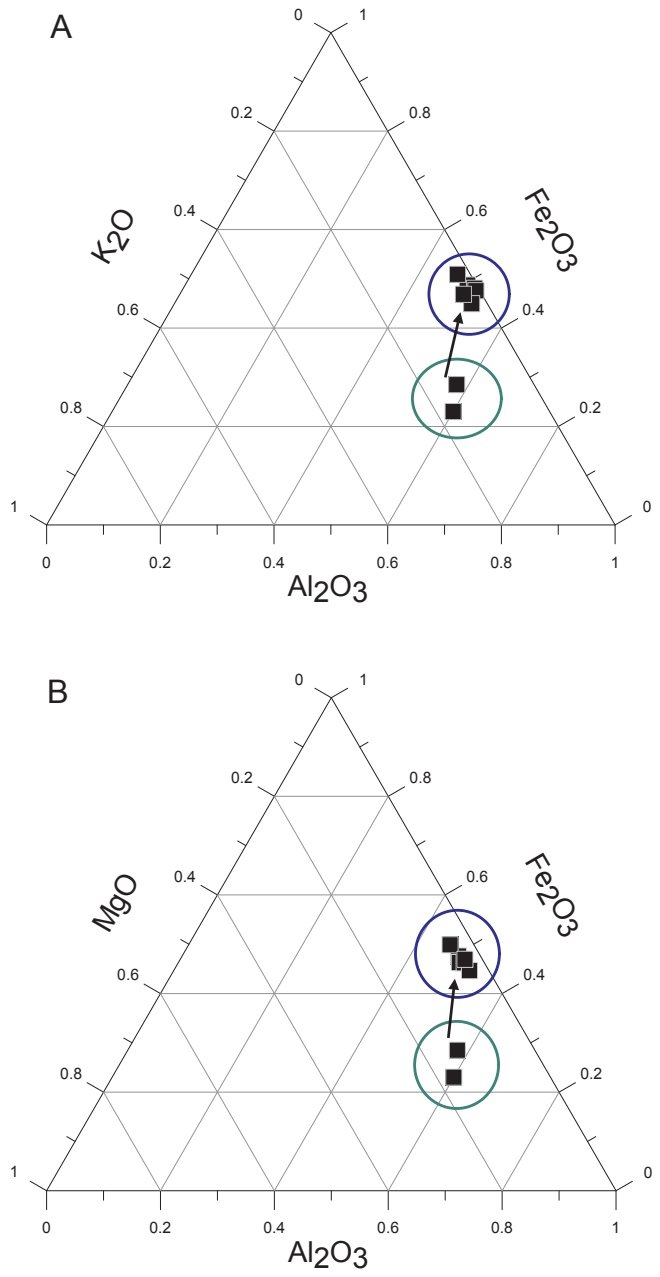

Fig. 9. Ternary plots designed from bulk chemical composition (ICP-OES data, Table 3). A – Ternary plot for Al_2O_3-Fe_2O_3-K_2O normalized data. B – Ternary plot for Al_2O_3-Fe_2O_3-MgO normalized data. The green circle contains the two samples from Saline-Sodic soils, Salina lake, with highest Fe-illite/glauconite layers content. The blue circle contains the samples Sodic and Solod soils, from Carandazal and Banhado lakes, with increase contents of smectite and kaolinite layers in the different MLM. The arrow indicates the direction of geochemical transformation due to freshwater inputs in the lakes.

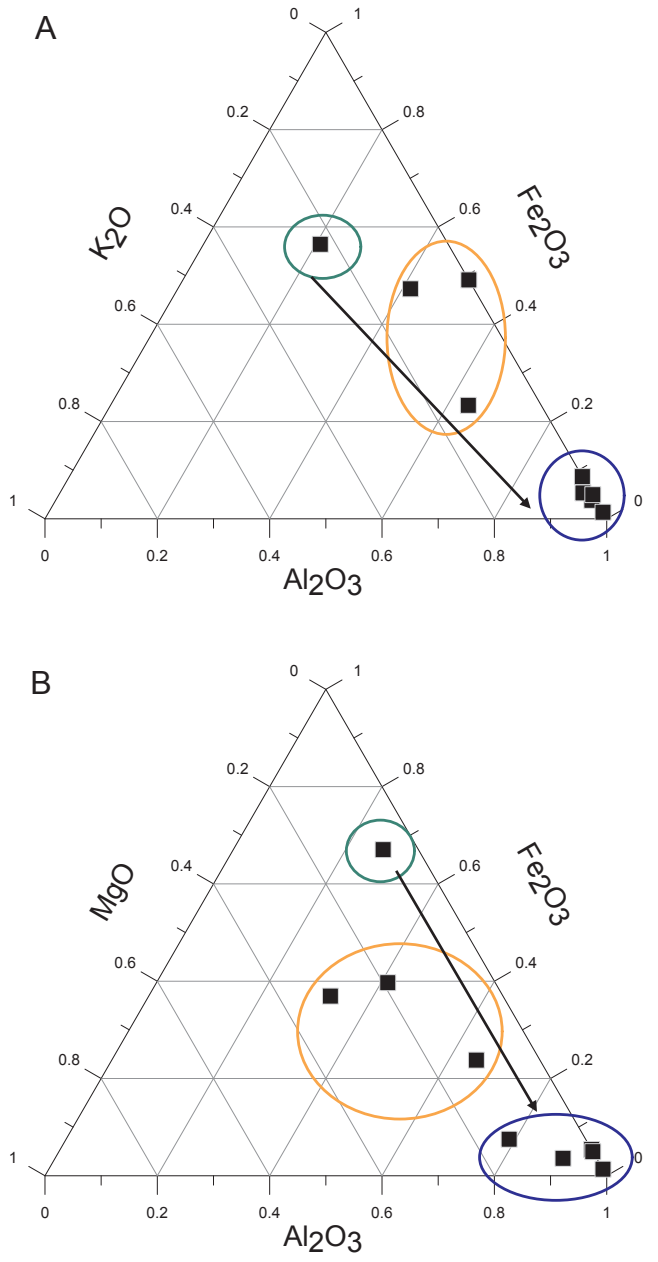

Fig. 10. Ternary plots designed from the chemical characterization of individual clay crystals (STEM data, Table 4). A – Ternary plot for Al_2O_3-Fe_2O_3-K_2O normalized data. B – Ternary plot for Al_2O_3-Fe_2O_3-MgO normalized data. The green circle contains the only crystal with illitic composition. The orange circle contains the crystals with smectititic composition (likely I-S). The blue circle contains the crystals with kaolinitic composition (kaolinite and K-S). The arrow indicates the progressive chemical change from illitic to kaolinitic composition.

position, as in the case of K^+. The ternary plot containing Al_2O_3-Fe_2O_3-MgO data (from STEM, Fig. 10B) indicates that Mg^{2+} is progressively lost due to action of acidic waters leading to cation depletion and kaolinite formation from the 2:1 clays (Dudek et al., 2006; Ryan and Huertas, 2009). However, since Mg^{2+} remains in the interlayer sites of smectite layers, the pathway of Mg^{2+} loss is more gradual than that of K^+. Smectitic crystals present higher Mg^{2+} content than illitic crystals, probably as an exchangeable cation. Some kaolinitic crystals still present residual Mg^{2+} (Table 4), emphasizing this difference when compared to K^+.

The 2:1 clays formed in hypersaline/alkaline environments, such as the Salina do Meio lake, usually present high octahedral Fe content, because these environments are also affected by variations in redox potential that drive oxidation/reduction cycles in Fe-oxyhydroxides and in clays (Huggett and Cuadros, 2005; Stanjek and Marchel, 2008; Furquim et al., 2010a; Andrade et al., 2018). The high Fe content in the only crystal assigned as illitic by STEM analysis confirms this trend, corroborating the Fe-illite/glauconite composition, which is consistent with XRD data and the results obtained by Furquim et al. (2010a) for Saline-Sodic soils. However, there were no significant correlations between the Fe_2O_3 values (ICP-OES data) or any of the three different types of clay layers distributed in the different minerals because this

element is not constrained to one type of layer in the different MLM (see Fe distribution in the different clay crystals, STEM data, Fig. 6).

On the other hand, the ternary plots designed with ICP-OES data show that Saline-Sodic samples (Salina lake) present a distinct high Fe content (Fig. 9A and B), endorsing the progressive "aluminization" of octahedral layers in clays as acidification of lakes takes place (in Carandazal and Banhado lakes). This "aluminization" is mainly related to kaolinitic crystals, as shown by the ternary plot containing STEM data (Fig. 10A and B), where the decrease in Fe content is very clear in these crystals. This depletion probably occurs together with Fe^{2+} oxidation to Fe^{3+}, because it promotes the reduction in layer charge when Fe-rich illite/glauconite transforms into vermiculite or smectite (Skiba et al., 2014; Kiesel et al., 2018). However, our chemical data do not allow the direct assessment of this mechanism.

5. Conclusion

The progressive evolution of salt-affected soils observed in the surroundings of the studied lake systems, provoked by freshwater input, induces clear sequential transformations in the clay minerals of the fine clay fraction. The sequential reactions involve the formation of MLM as transitory phases among the different clay types, as progressive acidification and cation leaching advance in the affected soil systems.

The Saline-Sodic soils, associated with a strongly alkaline system and submitted to both salinization and solonization, have illite-rich K-I phase (with more than 90% of Fe-rich/glauconite layers) as the main clay mineral. The illitic layers are partially replaced by kaolinite and smectite layers in the Sodic soils that undergo solonization, expressed in discrete kaolinite, I-V, K-I (rich in kaolinite layers) and K-S phases. In the Solods, which are associated with the most acidified system and have already been submitted to solodization, the percentages of illite are the lowest of the studied samples, being replaced by smectite and kaolinite layers, especially in K-S and discrete kaolinite phases.

The progressive geochemical and pedological changes were also observed in the Bnc1, Bnc2 and Bc horizons, which represent different stages of Bnq transformation from the Saline-Sodic soil. Thus, Bnc1 tended to present higher amounts of illite from the Sodic soils, in agreement with its higher morphological and chemical similarities with Bnq, such as strong green colors, alkaline pH values and high PST. On the other hand, the Bc horizon presented the lowest percentages of illite and the highest percentages of smectite layers from the Solods, corroborating its lower morphological and chemical similarities to Bnq, such as brownish colors and low pH and PST.

The range of structural and chemical compositions observed in the samples suggests that transformation from one clay mineral into another takes place without complete dissolution followed by the precipitation of the products, but as a progressive mixed-layering reaction. This model explains the existence of several MLM detected by the XRD full profile modelling procedure, which is in agreement with the chemical evolution of soils under progressive solonization and solodization. This is the first report of a pathway of clay mineral transformations in soils undergoing solonization and solodization in tropical environments and a rare register of the detailed evolution of clays in different salt-affected soils, which may have important implications for understanding the changes in mineralogical properties of soils dominated by 2:1 clay minerals under progressive acidification.

Declaration of Competing Interest

The authors declare that they have no known competing financial interests or personal relationships that could have appeared to influence the work reported in this paper.

Acknowledgments

The authors thank Fundação de Amparo à Pesquisa do Estado de São Paulo (FAPESP, Brazil) for the financial support to the research (grant number 2011/22491-0) and for the fellowship to A.C.B., Coordenação de Aperfeiçoamento de Pessoal de Nível Superior (CAPES, Brazil) for the fellowship to T.T.V.N, CNPq (Conselho Nacional de Desenvolvimento Científico e Tecnológico, Brazil) for the fellowship to G.C.S and G.R.C.. We also thank to: the Laboratório de Caracterização Estrutural of Universidade Federal de São Carlos (São Carlos, Brazil) by the use of STEM instrument and laboratory facilities (FAPESP grant number 09/53929-1; Financiador de Inovação e Pesquisa – FINEP, grant number 1359/06); the technicians of UNIFESP (Diadema), for help with the laboratory work; and the employees of the Nhumirim Farm (EMBRAPA) for their assistance in the field works.

Appendix A. Supplementary data

Supplementary data to this article can be found online at https://doi.org/10.1016/j.geoderma.2020.114380.

References

Aldega, L., Cuadros, J., Laurora, A., Rossi, A., 2009. Weathering of phlogopite to beidellite in a karstic environment. Am. J. Sci. 309, 689–710.
Alfonsi, R.R., Camargo, M.B.P., 1986. Condições climáticas para a região do Pantanal Matogrossense. Anais do 1o Simpósio sobre Recursos Naturais e Sócio-Econômicos do Pantanal, Corumbá, pp. 29–42 (in Portuguese).
Almeida, T.I.R., Sígolo, J.B., Fernandes, E., Queiroz Neto, J.P., Barbiero, L., Sakamoto, A.Y., 2003. Proposta de classificação e gênese das lagoas da baixa nhecolândia-MS com base em sensoriamento remoto e dados de campo. Rev. Brasil. Geociê. 33, 88–90 (in Portuguese).
Amouric, M., Olives, J., 1998. Transformation mechanisms and interstratification in conversion of smectite to kaolinite: an HRTEM study. Clay. Clay Miner. 46, 521–527.
Anderson, J.U., 1963. An improved pretreatment for mineralogical analysis of samples containing organic matter. Clay. Clay Miner. 10, 380–388.
Andrade, G.R.P., Azevedo, A.C., Lepchak, J.K., Assis, T.C., 2019. Weathering of Permian sedimentary rocks and soil clay minerals transformations under subtropical climate, southern Brazil (Paraná State). Geoderma 336, 31–48.
Andrade, G.R.P., Cuadros, J., Partiti, C.M., Cohen, R., Vidal-Torrado, P., 2018. Sequential mineral transformation from kaolinite to Fe-illite in two Brazilian mangrove soils. Geoderma 309, 84–99.
Antipov, I.K., Antipov, V.I., 1995. The role of clay minerals in the genesis of low-sodium Solonetz soils. Eurasian Soil Sci. 9, 1137–1140.
Arshad, M.A., Pawluk, S., 1966. Characteristics of some Solonetzic soils in the glacial lake Edmonton Basin of Alberta. II Mineralogy. J. Soil Sci. 17, 48–55.
Assine, M.L., Soares, P.C., 2004. Quaternary of the Pantanal, west-central Brazil. Quatern. Int. 114, 23–34.
Assine, M.L., 2003. Sedimentação na Bacia do Pantanal Mato-Grossense, Centro-Oeste do Brasil. Instituto de Geociências e Ciências Exatas, Universidade Estadual de São Paulo, Thesis, 106 p. (in Portuguese).
Assine, M.L., 2015. Brazilian Pantanal: a large pristine tropical wetland. In: Vieira, B.C., Salgado, A.A.R., Santos, L.J.C. (Eds.), Landscapes and Landforms of Brazil. Springer, pp. 135–146.
Balbino, M.A., 2017. Gênese de solos afetados por sais no entorno de uma lagoa salobra no Pantanal da Nhecolândia, Mato Grosso do Sul. Master thesis, Universidade de São Paulo (USP), 148 p. (in Portuguese).
Barbiero, L., Furian, S., Queiroz Neto, J.P., Ciornei, G., Sakamoto, A.Y., Capellari, B., Fernandes, E., Valles, V., 2002. Geochemistry of water and ground water in the Nhecolândia, Pantanal of Mato Grosso, Brazil: variability and associated processes. Wetlands 22, 528–540.
Barbiero, L., Rezende Filho, A., Furquim, S.A.C., Furian, S., Sakamoto, A.Y., Valles, V., Graham, R.C., Fort, M., Ferreira, R.P.D., Queiroz Neto, J.P., 2008. Soil morphological control of hydrogeochemistry in a saline and freshwater lake landscape in the Pantanal of Nhecolândia, Brazil. Geoderma 148, 91–106.
Bohn, H.L., McNeal, B.L., O'Connor, G.A., 2001. Soil Chemistry. John Wileyand Sons, 3rd edition, New York, 322 p.
Brunelle, A., Pawluk, S., Peters, T.W., 1976. Evaluation of profile development of some Solonetzic soils of south central Alberta. Can. J. Soil Sci. 56, 149–158.
Buey, S., Suarez Barrios, M., Garcia Romero, E., Dominguez Dias, M.C., Doval Montoya, M., 1998. Electron microscopic study of the illite– smectite transformation in the bentonites from Cerro del Aguila (Toledo, Spain). Clay Miner. 33, 501–510.
Carvalho, N.O., 1986. Hidrologia da Bacia do Alto Paraguai. Anais do 1o Simpósio sobre Recursos Naturais e Sócio-Econômicos do Pantanal, Corumbá, pp. 63–76. (in Portuguese).
Chizhikova, N.P., Khitrov, N.B., 2016. Diversity of clay minerals in soils of solonetzic complexes in the southeast of Western Siberia. Eurasian Soil Sci. 49, 1419–1431.
Collischonn, W., Tucci, C.E.M., Clarke, R.T., 2001. Further evidence of changes in the hydrological regime of the River Paraguay: part of a wider phenomenon of climate

change? J. Hydrol. 245, 218–238.
Deocampo, D.M., Cuadros, J., Wing-Dudek, T., Olives, J., Amouric, M., 2009. Saline lake diagenesis as revealed by coupled mineralogy and geochemistry multiple ultrafine clay phases: Pliocene Olduvai Gorge, Tanzania. Am. J. Sci. 309, 834–868.
Dong, H., Peacor, D.R., Murphy, S.F., 1998. TEM study of progressive alteration of igneous biotite to kaolinite throughout a soil profile. Geoch. Cosmochim. Acta 62, 1881–1887.
Dudek, T., Cuadros, J., Fiore, S., 2006. Interstratified kaolinite-smectite: nature of the layers and mechanism of smectite kaolinization. Am. Mineral. 91, 159–170.
Dumon, M., Tolossa, A.R., Capon, B., Detavernier, C., Van Ranst, E., 2014. Quantitative clay mineralogy of a Vertic Planosol in southwestern Ethiopia: Impact on soils formation hypotheses. Geoderma 214, 184–196.
Evans, T.L., Costa, M., 2013. Landcover classification of the lower Nhecolândia subregion of the Brazilian Pantanal wetland using ALOS/PALSAR, RADARSAT-2 and NVISAT/ASAR imagery. Remote Sens Environ 128, 118–127.
Fanning, D.S., Fanning, M.C.B., 1989. Soil: Morphology, Genesis, and Classification. John Wiley & Sons, New York, pp. 395.
Fernandes, E., 2007. Organização especial dos componentes da paisagem da Baixa Nhecolândia – Pantanal de Mato Grosso do Sul. Universidade de São Paulo, Thesis (in Portuguese).
Freitas, J.G., Furquim, S.A.C., Aravena, R., Cardoso, E.L., 2019. Interaction between lakes' surface water and groundwater in the Pantanal wetland, Brazil. Environ. Earth Sci. 78, 139–154.
Furquim, S.A.C., Santos, M.A., Vidoca, T.T., Balbino, M.A., Cardoso, E.L., 2017. Salt-affected soils evolution and fluvial dynamics in the Pantanal wetland, Brazil. Geoderma 286, 139–152.
Furquim, S.A.C., 2007. Formação de Carbonatos e Argilominerais em Solos Sódicos no Pantanal Sul-Mato-Grossense. Universidade de São Paulo (USP) Thesis (in Portuguese).
Furquim, S.A.C., Barbiéro, L., Graham, R.C., Queiroz Neto, J.P., Ferreira, R.P.D., Furian, S., 2010a. Neoformation of micas in soils surrounding an alkaline-saline lake of Pantanal wetland, Brazil. Geoderma 158, 331–342.
Furquim, S.A.C., Graham, R.C., Barbiero, L., Queiroz Neto, J.P., Vidal-Torrado, P., 2010b. Soil mineral genesis and distribution in a saline lake landscape of the Pantanal Wetland, Brazil. Geoderma 154, 518–528.
Furquim, S.A.C., Graham, R., Barbiero, L., Queiroz Neto, J.P., Vallès, V., 2008. Mineralogy and genesis of smectites in an alkaline-saline environment of Pantanal wetland, Brazil. Clay. Clay Miner. 56, 580–596.
Galán, E., Ferrel, R.E., 2006. Genesis of Clay Minerals. In: Bergaya, F., Lagaly, G (eds). Handbook of Clay Science. Part A: Fundamentals. Elsevier, Amsterdam, 2nd Ed., p. 83-126.
Gardi, C., Angelini, M., Barceló,S., Comerma, J., Gaistardo, C., Encina Rojas, A., Krasilnikov, P., Mendonça Santos Brefin, M.L., Montanarella, L., Muniz Ugarte, O., Schad, P., Vara Rodriguez; M.I., Vargas, R. (eds.), 2014. Atlas de Suelos de America Latina y el Caribe, Comisión Europea- Oficina de Publicaciones de la Unión Europea, L-2995 Luxembourg, 176 p. (in Spanish).
Gedroiz, K.K., 1925. Soil absorbing complex and the absorbed soil cations as a basis of genetic soil classification. Nosovka Agricultural Experimental Station. 38 (Translation into English: S.A. Waksman).
Godoi Filho, J.D., 1986. Aspectos Geológicos do Pantanal Mato-Grossense e de sua Área de Influência. Anais do 1o Simpósio sobre Recursos Naturais e Sócio-Econômicos do Pantanal, Corumbá, pp. 63–76.
Hallsworth, E.G., Waring, H.D., 1964. Studies in Pedogenesis in New South Wales. VIII. An alternative hypothesis for the formation of the Solodized Solonetz of the Pilliga disctrict. J. Soil Sci. 15, 158–177.
Heck, R.J., Mermut, A.R., 1992. Genesis of Natriborolls (Solonetzic) in a close lake basin in Saskatchewan, Canada. Soil Sci. Soc. Am. J. 56, 842–848.
Hubert, F., Caner, L., Meunier, A., Ferrage, E., 2012. Unraveling complex < 2μm clay mineralogy from soils using X-ray diffraction profile modelling on particle-size subfractions: implications for soils pedogenesis and reactivity. Am. Mineral. 97, 384–398.
Hubert, F., Caner, L., Meunier, A., Lanson, B., 2009. Advances in the characterization of soil clay mineralogy using X-ray diffraction: from decomposition to profile fitting. Eur. J. Soil Sci. 60, 1093–1105.
Huggett, J.M., Cuadros, J., 2005. Low-temperature illitization of smectite in the late Eocene and early Oligocene of the Isle of Wight (Hampshire basin), U.K. Am. Mineral. 90, 1192–1202.
Huggett, J.M., Cuadros, J., 2010. Glauconite formation in lacustrine/palaeosol sediments, Isle of Wight (Hampshire Basin), UK. Clay Miner. 45, 35–49.
Jackson, M.L., 1985. Soil Chemical Analysis-Advanced Course. By author, Madison-Wisconsin, 895 pp.
Karathanasis, A.D., Hajek, B.F., 1983. Transformation of smectite to kaolinite in naturally acid soil systems: structural and thermodynamic considerations. Soil Sci. Soc. Am. J. 47, 158–163.
Kiesel, M., Skiba, M., Skoneczna, M., Maj-Szeliga, K., Blachowski, A., 2018. Weathering of glauconite in an alkaline environment – a case study from Krakow area, Poland. Catena 171, 541–551.
Levy, G.J., Shainberg, I., Miller, W.P., 1998. Physical properties of Sodic soils. In: Sumner, M.E., Naidu, R. (Eds.), Sodic Soils, Distribution, Properties, Management, and Environmental Consequences. Oxford University Press, New York (USA), pp. 77–94.
Marcuzzo, F.F.N., Cardoso, M.R.D., Melo, D.C.R, 2010. Distribuição temporal da frequência de chuvas no bioma Pantanal. Anais do 3° Simpósio de Geotecnologias no Pantanal, Cáceres, Embrapa Informática Agropecuária/INPE, p. 160-169. (in Portuguese).
Marengo, J.A., Oliveira, G.S., Alves, L.M., 2016. Climate change scenarios in the Pantanal. In: Bergier, I., Assine, M.L. (Eds.) Dynamics of the Pantanal Wetland in South America. Springer International Publishing, pp. 227–238.
McBride, M.B., 1994. Environmental CHEMISTRY of SOILS. Oxford University Press, pp. 18 p..
Meunier, A., 2005. Clays. Springer-Verlag, Berlim, 472 p.
Monteiro, F.M., Fonseca, M.M., Madeira, M.A., Herbillon, A.J., 2012. Driven factors determining the occurrence of sodic soils in dry subhumid Mediterranean areas. J. Plant. Nutr. Soil. Sci. 175, 94–100.
Moore, D.M., Reynolds, R.C., 1997. X-Ray Diffraction and the Identification and Analysis of Clay Minerals, second ed. Oxford University Press, Oxford, pp. 378.
Newman, A.C.D., Brown G., 1987. The Chemical Constitution of Clays. In: Newman, A.C. D. (Ed.) Chemistry of Clays and Clay Minerals (Mineralogical Society Monograph No. 6), Longman Scientific & Technical, London, pp 1–128.
Odom, E., 1984. Glauconite and celadonite minerals. In: Bailey, S.W. (Ed.), Micas (Reviews in Mineralogy, 13). Mineralogical Society of America, pp. 545–573.
Oliveira Junior, J.C., Andrade, G.R.P., Barbiero, L., Furquim, S.A.C., Vidal-Torrado, P., 2019. Flooding effect on mineralogical changes in alkaline-sodic soil system of northern Pantanal wetlands, Brazil. Eur. J. Soil Sci. https://doi.org/10.1111/ejss.12871. In Press.
Padovani, C.R., 2010. Dinâmica espaço-temporal das inundações no Pantanal. Escola Superior de Agricultura Luiz de Queiroz (Esalq), Universidade de São Paulo (USP), Thesis. (in Portuguese).
Paquet, H., Bocquier, G., Millot, G., 1966. Néoformation et dégradation des minéraux argileux dans certains Solonetz Solodisés et Vertisols du Tchad. Bull. Serv. Carte Géol. Als. Lorr. 19, 295–322.
Parakshin, P.Y., 1984. Solonetzic soils of depressions of northern Kazakhstan. Soviet Soil Sci. 16, 9–16.
Pincus, L.N., Ryan, P.C., Huertas, F.J., Alvarado, G.E., 2017. The influence of soil age and regional climate on clay mineralogy and cation exchange capacity of moist tropical soils: a case study from Late Quaternary chronosequences in Costa Rica. Geoderma 308, 130–148.
Por, F.D., 1995. The Pantanal of Mato Grosso (Brazil) — World's Largest Wetlands. Klumer Ac. Publ. (122 p.).
Pott, A., Silva, J.S.V., 2016. Terrestrial and aquatic vegetation diversity of the Pantanal wetland. In: Bergier, I., Assine, M.L. (Eds.), Dynamics of the Pantanal Wetland in South America. Springer International Publishing, pp. 111–131.
Ryan, P.C., Huertas, F.J., 2009. The temporal evolution of pedogenic Fe-smectite to Fe-kaolin via interstratified kaolin-smectite in a moist tropical soil. Geoderma 151, 1–15.
Sandoval, F.M., Reichman, G.A., 1971. Some properties of Solonetzic (Sodic) soils in western North Dakota. Can. J. Soil Sci. 51, 143–155.
Santos, M.A., 2016. Caracterização e gênese de solos associados a uma lagoa salobra no Pantanal da Nhecolândia, Mato Grosso do Sul. Monography. Universidade Federal de São Paulo (UNIFESP), 58 p. (in Portuguese).
.Schaetzl, R.J., Anderson, S., 2005. Soils, Genesis and Geomorphology. Cambridge University Press, Cambridge, 817 p.
Silva, T.C., 1986. Contribuição da Geomorfologia para o Conhecimento e Valorização do Pantanal. Anais do 1o Simpósio sobre Recursos Naturais e Sócio-Econômicos do Pantanal Corumbá, pp. 77–90. (in Portuguese).
Skiba, M., Maj-Szeliga, K., Szymansky, W., Blachowski, A., 2014. Weathering of glauconite in soils of temperate climate as exemplified by a Luvisol profile from Góra Pulawska, Poland. Geoderma 235–236, 212–226.
Skoneczna, M., Skiba, M., Szymansky, W., Kiesel, M., Maj-Szeliga, K., Blachowski, A., 2019. Weathering of glauconite in alkaline soil of temperate climate: a case study from Górniki, eastern Poland. Geoderma 340, 146–156.
Sparks, D.L., 2003. Environmental Soil Chemistry, second ed. Academic Press, San Diego, U.S.A., pp. 351.
Spiers, G.A., Pawluk, S., Dudas, M.J., 1984. Authigenic mineral formation by solodization. Can. J. Soil Sci. 64, 5l5-532.
Stanjek, H., Marchel, C., 2008. Linking the redox cycles of Fe oxides and Fe-rich clay minerals: an example from a palaeosol of the Upper Freshwater Molasse. Clay Miner. 43, 69–82.
Tardy, Y., Bocquier, G., Paquet, H., Millot, G., 1973. Formation of clay from granite and its distribution in relation to climate and topography. Geoderma 10, 271–284.
Tarifa, J.R., 1986. O Sistema Climático do Pantanal: da compreensão do sistema à definição de prioridades de pesquisa climatológica. Anais do 1o Simpósio sobre Recursos Naturais e Sócio-Econômicos do Pantanal Corumbá, pp. 9–27. (in Portuguese).
USSL Staff, 1954. Diagnosis and Improvement of Saline and Alkali Soils. 60. U. S. Department of Agriculture, United States Salinity Laboratory (USSL), Washington Handbook, 160 p.
Velde, B., 1995. Origin and Mineralogy of Clays. Clays and the Environment. Springer, New York.
Vidoca, T.T.N., 2016. Análise de parâmetros morfológicos, granulométricos e químicos de solos associados a uma lagoa de água salobra no Pantanal da Nhecolândia, Corumbá-MS. Monography – Universidade Federal de São Paulo (UNIFESP). 126 p (in Portuguese).
Whittig, L.D., 1959. Characteristics and genesis of a Solodized Solonetz of California. Soil Sci. Soc. Am. Proc. 23, 469–473.
Zaidel'man, F.R., Ustinov, M.T., Pakhomova, E.Y., 2010. Solods of the Baraba Lowland and the Priobskoe Plateau: their properties and genesis and the methods of their diagnostics. Eurasian Soil Sci. 43, 1069–1082.
Zani, H., Assine, M.L., McGlue, M.M., 2012. Remote sensing analysis of depositional landforms in alluvial settings: method development and application to the Taquari megafan, Pantanal (Brazil). Geomorphology 161–162, 82–92.